# NDUFS2 (NADH:Ubiquinone oxidoreductase core subunit S2) in Mitochondrial Electron Transport Chain Complex I is Critical to Oxygen Responsiveness of Human Ductus Arteriosus Smooth Muscle Cells

Rachel E.T. Bentley[1], PhD, Kimberly J. Dunham-Snary[1,2], PhD, Ashley Y. Martin[1], Jeffrey D. Mewburn[2], Benjamin P. Ott[1], MSc, Bernard Thébaud[4-6], MD, PhD, Mark K. Friedberg[7], MD, PhD, Charles C.T. Hindmarch[1-3], PhD, Stephen L. Archer[1,3], MD

**Affiliations**

[1] Department of Medicine, Queen's University, Kingston, Ontario, Canada
[2] Department of Biomedical and Molecular Sciences, Queen's University, Kingston , Ontario, Canada
[3] Queen's Cardiopulmonary Unit, Translational Institute of Medicine, Department of Medicine, Queen's University, Kingston, Ontario, Canada
[4] Regenerative Medicine Program, Ottawa Hospital Research Institute, Ottawa, Ontario Canada
[5] Department of Cellular and Molecular Medicine, University of Ottawa, Ottawa, Ontario, Canada
[6] Neonatology, Department of Pediatrics, Children's Hospital of Eastern Ontario (CHEO) and CHEO Research Institute, Ottawa, Ontario, Canada
[7] Division of Cardiology, The Labatt Family Heart Center, Hospital for Sick Children and University of Toronto, Toronto, Ontario, Canada

**Short Title:** NDUFS2 is Critical to Oxygen Response of Human DA

**Corresponding Author:**
Stephen L Archer, MD, Department of Medicine, Queen's University, Kingston, Ontario, Canada. Queen's Cardiopulmonary Unit (QCPU), Room , BioSciences Complex. 116 Barrie St., Kingston, Ontario, Canada, K7L 3N6. Email: stephen.archer@queensu.ca

**Total Word Count: 8481/8000**

**Abstract**

**Rationale:** Mitochondria in ductus arteriosus (DA) smooth muscle cells (DASMC) are oxygen sensors that trigger $O_2$-induced vasoconstriction at birth; however, the molecular mechanisms of mitochondrial oxygen sensing are not fully understood. Many redox sensor proteins are conserved in the mammalian adult homeostatic oxygen sensing system, including NDUFS2 (NADH:Ubiquinone oxidoreductase core subunit S2), a component of mitochondrial Complex I that contributes to oxygen sensing in adult pulmonary arteries. Here we compared the role of NDUFS2 in DA oxygen sensing, to that of other Complex I subunits and putative $O_2$-sensor subunits, including: NADH:Ubiquinone oxidoreductase core subunit S1 (NDUFS1), NADH:Ubiquionone oxidoreductase core subunit S7 (NDUFS7), Ubiquinol-cytochrome c reductase, Rieske iron-sulfur polypeptide 1 (UQCRFS1), and Cytochrome c oxidase subunit 4I2 (COX4I2).

**Methods:** Human DASMC were grown in hypoxia (2.5% $O_2$, $pO_2$=41mmHg). Oxygen responsiveness of DASMC was assessed, measuring $O_2$-induced changes in intracellular calcium, $[Ca^{2+}]_i$, cell length, and mitochondrial reactive oxygen species (mROS) production. DASMC were treated for 48-hours with silencing RNA (siRNA) targeting NDUFS2, NDUFS1, NDUFS7, UQCRFS1, or COX4I2; knockdown was confirmed using qPCR and immunoblot. Mitochondrial metabolic consequences were assessed with micropolarimetry and Complex I, III, and IV activity assays. 3'RNA sequencing was used to explore the impact of gene knockdown on the DASMC molecular signature.

**Results:** The $O_2$-induced increase in $[Ca^{2+}]_i$ in siControl-treated cells (+18.6±2.3%) was reduced by siNDUFS2 (+5.5±1.5%, $p<0.0001$), but unchanged by other siRNAs. siNDUFS2 also uniquely depressed $O_2$-induced DASMC shortening (from -18.4±1.1% to -8.9±0.77%, $p<0.0001$), and mROS generation (+24±4.9% untreated versus -6.6±5.4% siNDUFS2, $p<0.0001$). The mitochondrial antioxidant MitoTEMPO also inhibited mROS (+2.9±4.5%, $p=0.001$) and attenuated oxygen-induced cell shortening (8.43±0.91%, $p=0.0003$). Knockdown of NDUFS2 and other ETC subunits did not inhibit mitochondrial respiration or ETC activity. Transcriptomics revealed unique changes in mitochondrial pathways with siNDUFS2.

**Conclusions:** NDUFS2 regulates mROS and acts as a mitochondrial oxygen sensor in human DASMC.

**Key Words:** Oxygen sensing, NADH:Ubiquinone oxidoreductase core subunit S1 (NDUFS1), NADH:Ubiquionone oxidoreductase core subunit S7 (NDUFS7), Ubiquinol-cytochrome c reductase, Rieske iron-sulfur polypeptide 1 (UQCRFS1), and Cytochrome c oxidase subunit 4I2 (COX4I2).

## 1. Introduction

The transition of the circulatory system from placental oxygenation in the fetus to an air-breathing neonate relies on the response of the ductus arteriosus (DA), a fetal vessel connecting the pulmonary artery and aorta. The acute functional constriction of the DA that occurs in the hours after birth triggered by the increase in arterial partial pressure of oxygen ($pO_2$), not only stops blood flow through the DA, terminating right-to-left shunting[1], but is a necessary precondition for permanent anatomical DA closure[2]. One of the most common complications of preterm birth, persistently patent ductus arteriosus (PDA) occurs when the DA fails to close[3,4]. PDA occurs in 55-70% of neonates with birth weight under 1000g and often causes hemodynamic compromise[5], with a prolonged postnatal left-to-right shunt associated with heart failure and numerous other complications[6]. Although our understanding of the DA oxygen response has increased, particularly our ability to manipulate closure using cyclooxygenase inhibitors like ibuprofen or meclofenamate[7], or using prostaglandins to maintain patency in ductus-dependent congenital heart diseases (DD-CHD)[8], the molecular identity of the DA oxygen sensor remains elusive and clinically relevant[9,10].

Despite the important role of the endothelium in DA closure, multiple groups have demonstrated endothelium-independent DA oxygen responses, suggesting that oxygen sensing primarily occurs in the DA smooth muscle (DASMC)[11]. Increased oxygenation and the onset of ventilation initiate a signaling cascade within DASMC, resulting in constriction. This cascade is initiated by increased mitochondrial-derived reactive oxygen species (mROS) generation, released by mitochondrial fission[12]. Mitochondrial ROS trigger a redox-mediated inhibition of voltage-gated potassium channels (Kv)[12]. Kv inhibition depolarizes the DASMC, increasing intracellular calcium concentration and inducing vasoconstriction (**Figure 1A-B**)[13]. This rapid ionic mechanism of DA constriction, occurring within seconds to minutes of birth and is ultimately reinforced by release of endothelial derived vasoconstrictors, like endothelin 1, and withdrawal of vasodilator prostaglandins, which are regulated at term to promote DA constriction[14,15].

The role of mitochondria as oxygen sensors in multiple specialized oxygen sensitive tissues, including the DA, pulmonary arteries, and carotid bodies, is well reported[16]. This collection of highly oxygen sensitive tissues that respond rapidly to physiologic changes in oxygenation is termed the homeostatic oxygen sensing system (HOSS) and functions to optimize systemic oxygen delivery[16]. The constriction of pulmonary arteries (PA) to hypoxia, a process known as hypoxic pulmonary vasoconstriction (HPV), enables ventilation-perfusion matching to optimize systemic oxygenation[17], while hypoxic stimulation of the carotid body type 1 (glomus) cells leads to neurosecretion and activation of the brainstem respiratory center[18], which increases ventilation and improves systemic oxygenation by increasing oxygen uptake from the environment[16]. There are conserved oxygen sensing mechanisms in all HOSS tissues, with oxygen-sensitive potassium channels mediating the responses of the DA, PA, and carotid body[13,18,19]. Mitochondria play a central role in the opposing oxygen responses of the DA and PA, the DA constricting to normoxia at birth versus the PA constricting to hypoxia. Inhibitors of ETC Complex I (rotenone) and Complex III (antimycin A) recapitulate the opposing response to hypoxia in DA and PA vascular rings and isolated SMC, relaxing the DA and constricting the PA[13,20,21]. This heterogeneity in mitochondrial signaling in response to changes in oxygen contrasts the downstream ionic effector pathway which are similar in DA versus PA, with Kv channel inhibitors causing concordant vasoconstriction, and L-type calcium channel inhibitors causing concordant vasodilation[13,22].

Complex I is a major site of mROS generation[23], with recent evidence supporting a key role for Complex I-specific mROS generation in mediating oxygen-induced DA constriction[24]. Specific subunits of ETC Complex I mediate oxygen responses of several HOSS tissues. Both Lopez-Barneo and our group have demonstrated that the Complex I subunit at the ubiquinone binding site ($I_Q$), NDUFS2 (NADH:ubiquinone oxidoreductase core subunit 2), is necessary for oxygen sensing of the carotid body glomus cells[25] and adult pulmonary arteries[26], respectively; however NDUF2's role in DASMC is uncertain. A unique role for NDUFS2 in constriction to oxygen in human DA is suggested by the RNAseq profile of human DASMC grown in hypoxia and then exposed to 3 days of normoxia, mimicking the fetal and neonatal oxygen conditions, respectively[27,28]. NDUFS2 was uniquely downregulated by oxygen exposure

amongst differentially expressed genes in Complex I, with expression of the other subunit I genes being upregulated[27].

Here we elucidate the contribution of various candidate ETC subunits to DA oxygen sensing by selectively knocking down NDUFS2 and other subunits using silencing RNA (siRNA) and examining the functional consequences (**Figure 1C**). We examined the contribution of other putative mitochondrial oxygen sensor subunits, which have been identified in adult PASMC and carotid bodies[29], but have not previously been assessed in fetal arteries, including the DA. These additional oxygen sensor candidate subunits studied include: the Rieske iron sulfur protein in complex III, encoded by *UQCRFS1* (Ubiquinol-Cytochrome C Reductase, Rieske Iron-Sulfur Polypeptide 1)[30], and Complex IV subunit *COX4I2* (Cytochrome C Oxidase Subunit 4I2)[31]. We also investigated NDUFS7, a Complex I subunit in the $I_Q$ site adjacent to NDUFS2, and NDUFS1, a Complex I subunit at the NADH binding site. Comparing effects of NDUFS2 knockdown to knockdown of subunits elsewhere within Complex I allowed us to determine if flow of electrons from NADH through Complex I (NDUFS1) or general inhibition of the ubiquinone binding site (NDUFS7) explain the inhibitory effects seen with siNDUFS2. Our findings support a unique role for NDUFS2 as an $O_2$ sensor in human DASMC (hDASMC).

## 2. Materials & Methods

Comprehensive descriptions of materials and methodology are included in the supplementary materials. Queen's University ethics approval was obtained from the Health Sciences and Affiliated Teaching Hospitals Research Ethics Board (HSREB) for the continued use of patient-derived human DASMC lines (TRAQ#6007784).

## 3. Results

Ten primary human DASMC cell lines, each with documented responsiveness to oxygen, were used for all *in vitro* studies. The demographics of the 10 infants from whom the DASMC were isolated are shown in **Table S2**.

### 3.1. Knockdown Optimization

Silencing RNAs (siRNA) targeting *NDUFS1*, *UQCRFS1*, and *COX4I2* were selected based on prior work in pulmonary artery SMC (PASMC)[26], with the *COX4I2* siRNA modified, based on alignment to known human gene sequences. Multiple siRNA targeting *NDUFS2* and *NDUFS7* were screened to determine the most effective siRNA (**Figure S1A-C**). The optimal time-point to measure endpoints after siRNA administration was experimentally determined based on depression of protein expression, assessed by immunoblot, measured 24, 48, and 72 hours post-siRNA. All protein expression was normalized to b-actin as a loading control, and expression was compared to both untreated (**Figure S1D-G, left**) and siControl-treated cells (**Figure S1D-G, right**). Maximal knockdown was achieved at 48-hours in hDASMC treated with siNDUFS1, siNDUFS2, and siUQCRFS1 (**Figure S1D-F**). In siCOX4I2 treated cells, there was a 38-58% knockdown at 48-hours of treatment, with a further reduction to 13-23% knockdown at 72-hours (**Figure S1G**). For consistency, all endpoint experiments were conducted at 48-hours of treatment.

### 3.2. siRNA Treatment Significantly Knocked Down ETC Subunit mRNA and Protein Expression

All siRNA constructs significantly reduced their target at both mRNA and protein levels. siNDUFS1 significantly decreased expression of *NDUFS1* mRNA (**Figure 2A**, n=4 cell lines, 93.5% decrease p=0.0007) and protein (**Figure 2B-C**, n=7 cell lines, 58.4% decrease, p=0.0034). siNDUFS2 significantly reduced expression of *NDUFS2* mRNA (**Figure 2D**, n=6 cell lines, 94.3% decrease, p<0.0001) and protein (**Figure 2E-F**, n=7 cell lines, 87.8% decrease, p=0.0006). siNDUFS7 significantly reduced expression of *NDUFS7* mRNA (**Figure 2G**, n=6 cell lines, 98.2% decrease, p<0.0001) and protein (**Figure 2H-I**, n=6 cell lines, 75.6% decrease, p=0.0004). siUQCRFS1 significantly reduced expression of *UQCRFS1* mRNA (**Figure 2J**, n=6 cell lines, 92.8% decrease, p=0.0014) and protein (**Figure 2K-L**, n=7 cell lines, 93.9% decrease, p<0.0001). siCOX4I2 significantly reduced expression of *COX4I2* mRNA (**Figure 2M**, n=3 cell lines, 90.1% decrease p=0.036) and protein (**Figure 2N-O**, n=5 cell lines, 51.2% decrease p=0.0077).

### 3.3. Knockdown of NDUFS2 Significantly Inhibits Oxygen Responsiveness of hDASMC

Oxygen responsiveness, defined as a rise in $[Ca^{2+}]_i$ within 20 minutes of oxygen exposure in DASMC loaded with the calcium-sensitive dye Cal-520AM, was assessed via confocal imaging (**Figure 3A left and middle**). Challenge with 80mM KCl served as a positive control, stimulating the maximal possible rise in intracellular calcium (**Figure 3A right**). KCl-induced increases in intracellular calcium were unaffected by any siRNA treatment (**Figure S2A-B**, n=1 representative cell line, 10-20 cells per cell line). Across n=10 cell lines, normoxia increased $[Ca^{2+}]_i$ 18.6±2.3% in untreated cells (**Figure 3B**), with no significant difference between untreated and siControl cells (16.0±1.9%, p>0.9999). In contrast, siNDUFS2-treated cells had only a 5.5±1.5% increase in $[Ca^{2+}]_i$ (p<0.0001), versus hypoxic baseline. The knockdown of NDUFS2 had no effect on KCl-induced increases in $[Ca^{2+}]_i$, indicating that siNDUFS2 specifically inhibited the DASMC oxygen response. There was a concomitant reduction of oxygen-induced DASMC shortening with siNDUFS2 (**Figure 3C, S2C-D**). Upon oxygen exposure, DASMC length in n=10 cell lines decreased 18.4±1.1%, relative to the length in hypoxia; siNDUFS2 significantly reduced this oxygen-induced cell shortening (**Figure 3C,** 8.9±0.7%, p=0.0009).

### 3.4. Oxygen-Induced Generation of Mitochondrial ROS is Inhibited by siNDUFS2

Oxygen-induced generation of mROS was assessed with live confocal imaging using the dye MitoROS™ 580 (n=10 cells per cell line, n=4 cell lines) to examine an early step in the DASMC oxygen response pathway (**Figure 1B**). There was a 24±4.9% increase in mitoROS fluorescence intensity upon exposure of untreated cells to normoxia (**Figure 3D-E**, 1456±57.6 to 1807±80.95 AU, p=0.0004). Pre-treatment with a mitochondrially-targeted antioxidant (MitoTEMPO) reduced normoxia-induced mROS (**Figure 3D-E**, to 1475±56.63 AU, p=0.001), as did knockdown of NDUFS2 (**Figure 3D-E**, to 1340±75.96 AU, p<0.0001). While MitoTEMPO significantly reduced mROS, a residual increase was still detected upon reoxygenation (**Figure 3E**, 1238±49.39 to 1475±58.63 AU, p=0.049); although statistically significant, this rise was markedly attenuated and did not exceed baseline mROS levels observed in untreated hypoxic cells.

siNDUFS2 also reduced $O_2$-induced DASMC shortening (**Figure 3F**, from 17.19±0.91% to 6.22±1.5% shortening, p=0.0001). Likewise, inhibiting mROS generation with MitoTEMPO attenuated oxygen-induced DASMC shortening (**Figure 3F**, from 17.19±0.91% to 8.43±0.91%, p=0.0005).

### 3.5. Knockdown of ETC Subunits, with the Exception of NDUFS1, Did Not Alter Complex I, III, and IV Activity

Activity of Complex I was measured by oxidation of NADH by dipstick-immunocaptured Complex I (**Figure 4A**). Complex I activity of hDASMC (n=8 cell lines) treated with siRNA targeting NDUFS2, NDUFS7, UQCRFS1, and COX4I2 was not significantly different than siControl-treated cells (**Figure 4B**). Knockdown of NDUFS1 significantly reduced Complex I activity, as expected per the assay's design, reported as signal intensity in arbitrary units (AU): siControl=2287±250, siNDUFS1=1775±199, p=0.024.

Complex III activity was measured as the change in concentration of reduced cytochrome c over time, measuring a linear subset within a recorded 10-minute period (**Figure S3A**). Complex III activity was calculated based on a standard curve (not shown), subtracting the change in concentration of reduced cytochrome c, over time, in samples treated with Antimycin A (**Figure S3B**). Activity of Complex III in hDASMC (n=5 cell lines) treated with siRNA targeting NDUFS1, NDUFS2, NDUFS7, UQCRFS1, COX4I2, or siControl was not significantly different (p=0.38) from activity in cell lines grown for 48-hours without siRNA (**Figure 4C**).

The activity of Complex IV was determined colorimetrically, measuring the change in absorbance at 550 nm to follow the oxidation of reduced cytochrome c and subtracting the background absorbance slope (**Figure S3C**). Across n=8 hDASMC cell lines, there was no significant change (p=0.58) in Complex IV activity with knockdown of NDUFS1, NDUFS2, NDUFS7, UQCRFS1, or COX4I2, compared to siControl treated cells (**Figure 4D**), indicating that ETC subunit knockdown did not impair the overall function of Complexes I, III, or IV.

### 3.6. ETC Subunit Knockdown Did Not Alter Mitochondrial Metabolic Function

Whole cell mitochondrial metabolism was assessed with micropolarimetry using the Seahorse Mito Stress Test (**Figure S4A**) with an experimentally optimized concentration of FCCP (**Figure S4B**). Treatment of hDASMC (n=6 cell lines) with siRNA for 48-hours did not significantly change key mitochondrial metabolic parameters (**Figure 5A**), including basal respiration (**Figure 5B**), spare respiratory capacity (**Figure 5C**). and ATP-linked respiration (**Figure 5D**). There was similarly no effect of any ETC subunit knockdown on other derived mitochondrial metabolic parameters (**Figure S4C-G**).

### 3.7. Knockdown of ETC Subunits Induced Widespread Transcriptomic Changes, with NDUFS2 Knockdown inducing a Robust Change in Mitochondrial Phenotype

Treatment of hDASMC (n=5 cell lines) with siRNA targeting NDUFS2, NDUFS1, NDUFS7, UQCRFS1, or COX4I2 for 48-hours induced substantial transcriptomic changes compared to siControl, as assessed via 3'RNA sequencing. There were 677 DEGs commonly regulated between siControl and ETC knockdowns that were found independent of which subunit was knocked down (**Figure 6A, Figure S5**).

To compare the effects of siNDUFS2 to other ETC knockdowns, we examined the log fold change of each knockdown versus siControl for the top 20 DEGs between siNDUFS2 and siControl (**Figure 6B**). siNDUFS2 exhibited a distinct phenotype among knockdown conditions, uniquely downregulating *NDUFS2*, *FGF16*, *AFRIP1*, *CDK17*, *KIF3B*, and *LIPA*, and uniquely upregulating of *ZMAT3* and *ANKRD13C-DT*, as discussed below (**Figure 6B**). Of these 20 DEGs, there was also a common effect of ETC subunit knockdowns on expression of genes, such as the histone-binding *CBX1* and *DNM1L*, the gene encoding DRP1, the major mediator of mitochondrial fission. There was also a shared effect of some knockdown conditions on expression of the phosphoserine aminotrasferase *PSAT1*, *SNAR-E*, a non-coding small nuclear RNA (snRNA), and *HMMR*, a hyaluronic acid receptor involved in cell motility **(Figure 6B**).

Knockdown of NDUFS2 uniquely regulated the expression of 578 genes relative to siControl (**Figure 6A**), meaning these changes were not seen with siRNA targeting other subunits. Gene ontology (GO) analysis of these unique 578 genes revealed enrichment of pathways related to mitochondrial structure and functions (**Figure 7A-C**).

## 4. Discussion

We previously identified downregulation of NDUFS2 mRNA in hDASMC in response to normoxia[27,28]. Here, the functional contribution of candidate ETC subunits to oxygen-induced hDASMC constriction was interrogated to determine the contribution of ETC subunits, including NDUFS2 and other putative sensor subunits of other HOSS tissues, to oxygen sensing of hDASMC. We examined the functional effects of ETC subunit knockdown, while also performing an RNAseq analysis to establish the transcriptomic impact of these genes, demonstrating that NDUFS2 mediates the human DASMC's oxygen response. Only knockdown of NDUFS2 in hDASMC inhibited an oxygen-induced rise in intracellular calcium and decrease in cell length, surrogates for DA constriction *in vivo.* siNDUFS2 also largely attenuated the oxygen-induced rise in mROS in hDASMC, indicating that it likely blocked DASMC contraction by interfering with the mROS signaling mechanism. It is noteworthy that siNDUFS2 knockdown had no effect on KCl-induced rise in intracellular calcium, supporting the specificity of its effects for the response to oxygen. The inhibition of DA oxygen responsiveness occurring with knockdown of NDUFS2 is also shown to be independent of effects on mitochondrial metabolic function, with no change in mitochondrial respiration or ETC Complex I, III, or IV activity being observed. This suggests that NDUFS2 plays a vital, early role in oxygen-induced DA constriction through its ability to reduce the physiologic increase in mROS that occurs in response to increases in $pO_2$. Importantly we also demonstrated that these hDAMSC, isolated from infants at the time of congenital heart surgery, were indeed SMC and that, despite passage in hypoxic culture, they retained the classical DA oxygen responsive phenotype, manifesting as a rise in cytosolic calcium and contraction in response to physiologic oxygen concentrations, as occurs with the first breath[27].

Knockdown of other Complex I subunits, NDUFS1 and NDUFS7, did not affect oxygen responsiveness or mitochondrial respiration. Although, knockdown of NDUFS1 decreased proximal Complex I activity (i.e. NADH oxidation). NDUFS2, NDUFS1, and NDUFS7 are all highly conserved subunits, part of the 14 subunits of minimal Complex I assembly[32]. NDUFS2 and NDUFS7 are situated at the ubiquinone binding site ($I_Q$), where electrons are transferred to ubiquinone and where rotenone, the classical Complex I inhibitor, binds[33]. This $I_Q$ site is a major site of mROS generation in Complex I[34,35]; mROS generation from this site mediates rabbit DA closure *in vivo*[24]. The absence of effect of NDUFS7 knockdown on DA oxygen response indicates a unique role for NDUFS2 within the $I_Q$ site in oxygen sensing, altering mROS generation.

NDUFS1, in contrast, is in the peripheral arm of Complex I (**Figure 1**), part of the electron input/dehydrogenase (N) functional module of Complex I that accepts electrons via oxidation of NADH. While it is the prosthetic group flavin mononucleotide (FMN), and not NDUFS1 that directly accepts electrons from NADH[36], NDUFS1 plays a vital role in the function and stability of the N-module[37]. NDUFS1 is associated with multiple iron-sulfur (Fe-S) clusters in Complex I that are essential cofactors and mediate electron transfer in the respiratory chain, including Fe-S clusters N1b, N4, and N5[33,38]. A recent study demonstrated that biallelic mutation of NDUFS1 decreased the N-module stability and disrupted the flow of electrons between two Fe-S clusters (N4 and N5), impairing supercomplex formation in patient-derived skin fibroblasts[37]. With the contribution of NDUFS1 to the N-module structure and function, the inhibition of Complex I function that we observed with knockdown of NDUFS1 was expected, particularly as the assay measured activity based on NADH oxidation. However, the lack of effect of NDUFS1 knockdown on live cell mitochondrial respiration suggests respiratory chain function was maintained despite this knockdown.

It is well known that mROS in DASMC initiate the DA response to oxygen[13]. Complex I and III are the primary sites of mROS generation within the mitochondria[23], with the diffusible ROS (e.g. $H_2O_2$) serving as a redox messenger to alter the activity of Kv channels and thus the polarization/depolarization state of the DASMC membrane[20]. Similar to the effects seen in the adult PA[22], treatment of DASMC with classic inhibitors of both ETC Complex I (rotenone) and Complex III (antimycin A) mimics hypoxia[13]. However, these inhibitors not only stop the flow of electrons through the ETC thereby potentially eliminating mROS signaling molecules; they also suppress metabolism making it difficult to differentiate their effects on Complex I or III mROS generation from their bioenergetic and ETC inhibitory effects. Using the novel compound S1QEL (suppressor of site $I_Q$ electron leak)[39] to inhibit Complex I ROS generation without altering bioenergetics, oxygen-induced rabbit DA constriction was reversed *ex vivo* and rabbit DA closure at birth was inhibited *in vivo*[24]. This response was unique to Complex I mROS, with no effect of inhibiting Complex III electron leak using S3QEL (suppressor of site $III_{Qo}$ electron leak)[40] on oxygen-induced rabbit DA constriction *ex vivo*, with preserved vasoconstriction to KCl and phenylephrine following both S1QEL and S3QEL treatment[24]. The current study advances that finding by identifying NDUFS2, situated in the $I_Q$ site of Complex I, as the primary source of oxygen-induced mROS generation in humans and demonstrating its key role in oxygen-induced DASMC constriction (**Figure 3D-F**).

Further supporting this conclusion, inhibition of mROS using the mitochondrial superoxide scavenger MitoTEMPO, at a concentration documented to decrease normoxic mROS levels, attenuates oxygen-induced cell shortening to a similar degree as NDUFS2 knockdown (**Figure 3F**). Together these results demonstrate that knockdown of NDUFS2 inhibits DASMC oxygen responsiveness via inhibition of mROS generation within ETC Complex I. These results align with the current literature, further supporting the paradigm that the DASMC oxygen response results from oxygen-induced increases in mROS from Complex I[11,13,24].

Complex III mROS generation has not been intensively studied in DA oxygen sensing (although we found no effect of S3QEL on DA constriction in rabbits); however, it is not clear whether Complex I or III is most responsible for initiating hypoxic pulmonary vasoconstriction (HPV)[26,30]. Based on this disagreement, as well as the known hypoxia mimicking effect of antimycin A[13], we sought to determine

any possible role of Complex III in the DA oxygen response by knocking down the Rieske Fe-S cluster. Successful knockdown of UQCRFS1 (confirmed at the protein level) had no effect on oxygen responsiveness, mitochondrial respiration, or ETC Complex activity (similar to our previous observations in adult PASMC), arguing against an important role for complex III in the human DASMC's oxygen response.

Our examination of Complex IV subunit COX4I2 was similarly based on evidence that it may contribute to oxygen-sensing (HPV) in adult PAs[16]. Complex IV catalyzes the final step of the ETC, receiving the terminal electron from the ETC and converting oxygen to water. COX4I2 modulates Complex IV activity and thus ETC activity[31]. Sommer *et al.* demonstrated impaired HPV in adult COX4I2 knockout mice[31], though Dunham-Snary *et al.* found no effect of siCOX4I2 on HPV in adult rats[26]. Our incomplete knockdown of COX4I2, was consistent with previously reported levels (~55% knockdown)[26]; siRNA dose was not increased because complete *COX4I2* knockdown would likely interfere with the function of other ETC Complexes[41,42]. The ETC Complexes I-IV interact and form large structures termed supercomplexes[43], with an interdependence of complex biogenesis and/or stability, particularly that of Complex I[44-46]. Deficiencies in Complex III[44,45] or IV[41,47] greatly decrease assembled Complex I in monomeric and supercomplex form. With 51.2±13% knockdown of COX4I2 protein seen in our cells, there was no significant effect on mitochondrial respiration or activity of Complex I, III, or IV. There was also no evidence of COX4I2 contributing to the oxygen response of human DASMC.

While only NDUFS2 knockdown attenuated DASMC oxygen responsiveness, transcriptomics revealed that all knockdowns regulated DASMC gene expression, with 677 common DEGs between all knockdown conditions versus siControl (**Figure 6A**). GO pathway analysis reveals commonly regulated genes relate to generic cellular processes (**Figure S5A-C**) with no clear mitochondrial phenotype emerging as common amongst all ETC knockdowns.

The RNA sequencing data also confirms that each knockdown was effective at reducing the expression of the target subunit genes without altering expression of mRNA for other candidate sensor subunits (**Figure S6A-E**). We were unable to detect COX4I2 in any siRNA condition in our RNA sequencing data (**Figure S6E**); however, we effectively knocked COX4I2 down at both the gene and protein level, and there was a clear effect of siCOX4I2 on other gene expression (**Figure 6A)**. 3' RNA sequencing captures only 75 base pairs from the 3' end of mRNA, so we hypothesize that seq reads aligned to a shared locus, rendering those reads to be unassigned or assigned to another gene. Others have observed a compensatory upregulation of COX4I2 with deficiency of the other COX4 isoform (COX4I1)[48], thus is it possible that this interdependent relationship could hold true in the opposite direction; we observed a non-significant increase in COX4I1 in cells treated with siCOX4I2, further suggesting that COX4I2 was effectively knocked down in our samples.

To compare the effects of the different ETC knockdowns on gene expression, we explored the 20 most differentially expressed genes that resulted from NDUFS2 knockdown across all knockdowns (**Figure 6B**). The genes uniquely upregulated by siNDUFS2 among knockdown conditions included ZMAT3, an RNA-binding protein vital to the p53 tumour suppression pathway[49] and the long non-coding RNA (lncRNA) ANKRD13C-DT. While there is no known specific function of ZMAT3 in the DA[50], disruption of another RNA-binding protein that affects splicing (Matrin3)[51] was associated with congenital heart defects, including PDA, in a patient and a mouse model[52], suggesting an important role for RNA binding proteins in DA anatomical closure. Additionally, p53 upregulates and activates the antiproliferative growth regulator CCN3[53], which inhibits DA intimal cushion formation[54]. Together these data suggest that ZMAT3 and the p53 pathway may play a role in DA remodeling, and that NDUFS2 knockdown may act on this axis to inhibit DA closure. This observation is relevant because initial DA constriction (which is blocked by siNDUFS2) is critical for subsequent DA anatomical closure[2].

ANKRD13C-DT (also known as HHLA3), which was upregulated by siNDUFS2, has been associated with worse prognosis in multiple solid tumors. Zhou et al. identified ANKRD13C-DT as a pyroptosis-related lncRNA in human lung adenocarcinomas that displayed a pro-proliferative role in lung

adenocarcinoma cells, with knockdown decreasing cell proliferation and increasing ROS generation[55]. Long non-coding RNAs have been linked to congenital heart diseases and associated lung diseases, including pulmonary arterial hypertension and bronchopulmonary dysplasia[56,57]. However, ANKRD13C-DT has not been identified as related to congenital heart diseases nor is it known to have a specific function in the DA, though its effects on ROS generation[55] may explain its upregulation with NDUFS2 knockdown. Furthermore, the effect of ANKRD13C-DT on proliferation may point to a potential role in permanent anatomical DA closure, suggesting a possible multifaceted connection between NDUFS2 manipulation and both functional and anatomical DA closure that merits future study.

Among the top 20 genes regulated by NDUFS2 knockdown, there was unique downregulation with siNDUFS2 of five genes. ARFIP1 and KIF3B are both involved in intracellular movement and transport, with ARFIP1 functioning in secretory granule biogenesis and exit from the *trans*-Golgi network[58,59], and KIF3B functioning in mitosis, meiosis, and transport of macromolecules[60]. CDK17 is an atypical cyclin-dependent kinase[61] and little is known about its physiological and pathological roles[62], though it is thought to be involved in the regulation of vesicle internalization and trafficking[62]. FGF16 is involved in embryonic development and induces cardiomyocyte proliferation[63], while LIPA plays a key role in lipid metabolism, hydrolyzing cholesterol and triglyceride esters in the lysosome[64]. These proteins do not have a known role in the pathophysiology of ductus arteriosus closure and oxygen sensing, though another lipase (LIPC) was associated with development of PDA[65] and CDK17 was identified in a meta-analysis by Yarboro *et al.* as being enriched in the DA versus aorta in rodents[66]. However, the function of CDK17 in the DA is unknown and the other genes have not been studied in the context of the DA. The downregulation of these genes with NDUFS2 knockdown may indicate a change in internalization and secretion of macromolecules and/or proliferation relating to DA closure, though the specific functions of these genes in the DA remain unknown.

Comparing the top 20 GO pathways in each domain of the DEGs unique to each knockdown condition, the enriched GO pathways for siNDUFS2 had a distinctly mitochondrial phenotype (**Figure 7A-C**). Of the top 20 most enriched GO pathways unique to the other ETC knockdowns (**Figures S7, S9, S11, S13**), the only mitochondrial GO term to appear is "mitochondrion" with siNDUFS1, as compared with the 14 mitochondrial GO terms appearing in the most enriched pathways with siNDUFS2. Searching for mitochondrial GO pathways enriched with NDUFS2 knockdown (**Figure 8**) also suggests a strong mitochondrial phenotype among DEGs, while the same search with other knockdown conditions (**Figure S8, S10, S12, S14**) revealed mitochondrial pathways that primarily contained only one or two genes, indicating few of the DEGs were related to mitochondria. GO analysis of the genes unique to NDUFS2 knockdown also revealed enrichment of nucleotide/nucleoside biosynthetic and binding pathways; these were similarly enriched by chronic normoxic exposure in human DASMC in our previous transcriptomic study, a study in which NDUFS2 was uniquely downregulated by normoxia, amongst all other Complex I subunits[27,28]. This indicates a similar effect of NDUFS2 knockdown and changing oxygen conditions to mimic fetal and neonatal environments[27]. The loss of NDUFS2 upon prolonged oxygen exposure may explain why the DA loses its ability to respond to oxygen in the days after initial closure.

We established a key function of NDUFS2 in the DA's oxygen response, though some questions remain. In some cell lines, there was a complete elimination of oxygen response with knockdown of NDUFS2 (**Figure S2E**); however, across the pooled data from n=10 human DASMC cell lines studied, while there was a significant inhibition, we did not see complete inhibition of oxygen-induced increase in intracellular calcium. This may reflect inter-individual differences in the importance of NDUFS2, as each cell line was from a different baby, with various congenital heart diseases and collected at different ages[27]. With limited patient data and a heterogeneous sample group it is difficult to conclude if NDUFS2 is the universal oxygen sensor of the DASMC or if other subunits also contribute to the DA's oxygen response in some infants. Future studies manipulating NDUFS2 in additional human whole DA and DASMC, as well as pharmacological manipulation in preclinical models, may further elucidate the role of NDUFS2 in DA oxygen sensing. As PDA is primarily a disease of prematurity, future studies should explore the maturational changes in NDUFS2 to examine its role in DA closure and PDA pathophysiology.

## 5. Conclusions

This first identification of NDUFS2 as the human DA oxygen sensor enhances our understanding of the molecular basis for the normal physiologic response of this vessel to the shift from a hypoxic fetal environment to a normoxic neonatal environment. Further exploration and manipulation of NDUFS2 and the oxygen sensing pathway may lead to improved modulation of DASMC constriction and thus DA patency. While current therapies are effective at maintaining DA patency in cases of ductus-dependent congenital heart diseases, cyclooxygenase inhibitors are ineffective in closing PDA in approximately 30% of cases, with much lower efficacy in infants born under 1000g[67]. Current pharmacologic therapy to close PDA is also associated with toxicity, including renal failure (11%), necrotizing enterocolitis (3%), and gut perforation (8%), further highlighting a need for advancement in treatments[68]. Targeting NDUFS2 in the DA oxygen sensing pathway may be a promising novel therapeutic strategy to close PDA or maintain DA patency in ductus-dependent congenital heart defects.

**Sources of Funding**
This work was supported by a grant from the Canadian Institutes for Health Research (CIHR 183762).

**Disclosures:** None

**Supplemental Material**
Supplemental Methods
Table S1-S2
Figures S1-S14

## 6. References


1. Jager BV, Wollenman OJ. An Anatomical Study of the Closure of the Ductus Arteriosus. *Am J Pathol*. 1942;18:595-613.
2. Clyman RI, Chan CY, Mauray F, Chen YQ, Cox W, Seidner SR, Lord EM, Weiss H, Waleh N, Evans SM, et al. Permanent anatomic closure of the ductus arteriosus in newborn baboons: the roles of postnatal constriction, hypoxia, and gestation. *Pediatr Res*. 1999;45:19-29. doi: 10.1203/00006450-199901000-00005
3. Egbe A, Uppu S, Stroustrup A, Lee S, Ho D, Srivastava S. Incidences and sociodemographics of specific congenital heart diseases in the United States of America: an evaluation of hospital discharge diagnoses. *Pediatr Cardiol*. 2014;35:975-982. doi: 10.1007/s00246-014-0884-8
4. Kitterman JA, Edmunds Jr LH, Gregory GA, Heymann MA, Tooley WH, Rudolph AM. Patent ductus arteriosus in premature infants: incidence, relation to pulmonary disease and management. *New England Journal of Medicine*. 1972;287:473-477.
5. Koch J, Hensley G, Roy L, Brown S, Ramaciotti C, Rosenfeld CR. Prevalence of spontaneous closure of the ductus arteriosus in neonates at a birth weight of 1000 grams or less. *Pediatrics*. 2006;117:1113-1121. doi: 10.1542/peds.2005-1528
6. Terrin G, Di Chiara M, Boscarino G, Metrangolo V, Faccioli F, Onestà E, Giancotti A, Di Donato V, Cardilli V, De Curtis M. Morbidity associated with patent ductus arteriosus in preterm newborns: a retrospective case-control study. *Italian Journal of Pediatrics*. 2021;47:1-8.
7. Heymann MA, Rudolph AM, Silverman NH. Closure of the ductus arteriosus in premature infants by inhibition of prostaglandin synthesis. *New England Journal of Medicine*. 1976;295:530-533.
8. Singh Y, Mikrou P. Use of prostaglandins in duct-dependent congenital heart conditions. *Archives of Disease in Childhood-Education and Practice*. 2018;103:137-140.
9. Maron JL. Patent Ductus Arteriosus—To Close or Not to Close? *Obstetric Anesthesia Digest*. 2024;44:100.
10. Buvaneswarran S, Wong YL, Liang S, Quek SC, Lee J. Active treatment vs expectant management of patent ductus arteriosus in preterm infants: a meta-analysis. *JAMA pediatrics*. 2025.
11. Bentley RE, Hindmarch CC, Archer SL. Using omics to breathe new life into our understanding of the ductus arteriosus oxygen response. *Seminars in Perinatology*. 2023;47:151715.
12. Hong Z, Kutty S, Toth PT, Marsboom G, Hammel JM, Chamberlain C, Ryan JJ, Zhang HJ, Sharp WW, Morrow E, et al. Role of dynamin-related protein 1 (Drp1)-mediated mitochondrial fission in oxygen sensing and constriction of the ductus arteriosus. *Circ Res*. 2013;112:802-815. doi: 10.1161/CIRCRESAHA.111.300285
13. Michelakis ED, Rebeyka I, Wu X, Nsair A, Thebaud B, Hashimoto K, Dyck JR, Haromy A, Harry G, Barr A, et al. O2 sensing in the human ductus arteriosus: regulation of voltage-gated K+ channels in smooth muscle cells by a mitochondrial redox sensor. *Circ Res*. 2002;91:478-486. doi: 10.1161/01.res.0000035057.63303.d1
14. Coceani F, Kelsey L. Endothelin-1 release from lamb ductus arteriosus; relevance to postnatal closure of the vessel. *Canadian journal of physiology and pharmacology*. 1991;69:218-221.
15. Coceani F, Olley PM. The response of the ductus arteriosus to prostaglandins. *Can J Physiol Pharmacol*. 1973;51:220-225. doi: 10.1139/y73-031
16. Weir EK, Lopez-Barneo J, Buckler KJ, Archer SL. Acute oxygen-sensing mechanisms. *N Engl J Med*. 2005;353:2042-2055. doi: 10.1056/NEJMra050002
17. Archer SL, Dunham-Snary KJ, Bentley RE, Alizadeh E, Weir EK. Hypoxic Pulmonary Vasoconstriction: An Important Component of the Homeostatic Oxygen Sensing System. *Physiological Research*. 2024;73:S493.
18. López-Barneo J, López-López JR, Ureña J, Gonzalez C. Chemotransduction in the carotid body: K+ current modulated by P O2 in type I chemoreceptor cells. *Science*. 1988;241:580-582.

19. Archer SL, Souil E, Dinh-Xuan AT, Schremmer B, Mercier J-C, El Yaagoubi A, Nguyen-Huu L, Reeve HL, Hampl V. Molecular identification of the role of voltage-gated K+ channels, Kv1. 5 and Kv2. 1, in hypoxic pulmonary vasoconstriction and control of resting membrane potential in rat pulmonary artery myocytes. *The Journal of clinical investigation*. 1998;101:2319-2330.
20. Archer SL, Wu X-C, Thébaud B, Moudgil R, Hashimoto K, Michelakis ED. O2 sensing in the human ductus arteriosus: redox-sensitive K+ channels are regulated by mitochondria-derived hydrogen peroxide. *Biol Chem*. 2004;385:205-216.
21. Archer SL, Huang J, Henry T, Peterson D, Weir EK. A redox-based O2 sensor in rat pulmonary vasculature. *Circulation research*. 1993;73:1100-1112.
22. Michelakis ED, Hampl V, Nsair A, Wu X, Harry G, Haromy A, Gurtu R, Archer SL. Diversity in mitochondrial function explains differences in vascular oxygen sensing. *Circ Res*. 2002;90:1307-1315. doi: 10.1161/01.res.0000024689.07590.c2
23. Forman HJ, Boveris A. Superoxide radical and hydrogen peroxide in mitochondria. In: *Free Radicals in Biology*. Academic Press Inc.; 1981:65-90.
24. Read AD, Bentley RE, Martin AY, Mewburn JD, Alizadeh E, Wu D, Lima PD, Dunham-Snary KJ, Thébaud B, Sharp W. Electron Leak From the Mitochondrial Electron Transport Chain Complex I at Site IQ Is Crucial for Oxygen Sensing in Rabbit and Human Ductus Arteriosus. *Journal of the American Heart Association*. 2023;12:e029131.
25. Fernandez-Aguera MC, Gao L, Gonzalez-Rodriguez P, Pintado CO, Arias-Mayenco I, Garcia-Flores P, Garcia-Perganeda A, Pascual A, Ortega-Saenz P, Lopez-Barneo J. Oxygen Sensing by Arterial Chemoreceptors Depends on Mitochondrial Complex I Signaling. *Cell Metab*. 2015;22:825-837. doi: 10.1016/j.cmet.2015.09.004
26. Dunham-Snary KJ, Wu D, Potus F, Sykes EA, Mewburn JD, Charles RL, Eaton P, Sultanian RA, Archer SL. Ndufs2, a Core Subunit of Mitochondrial Complex I, Is Essential for Acute Oxygen-Sensing and Hypoxic Pulmonary Vasoconstriction. *Circ Res*. 2019;124:1727-1746. doi: 10.1161/CIRCRESAHA.118.314284
27. Bentley RE, Hindmarch CC, Dunham-Snary KJ, Snetsinger B, Mewburn JD, Thébaud A, Lima PD, Thébaud B, Archer SL. The molecular mechanisms of oxygen-sensing in human ductus arteriosus smooth muscle cells: A comprehensive transcriptome profile reveals a central role for mitochondria. *Genomics*. 2021;113:3128-3140.
28. Bentley RET, Hindmarch CCT, Dunham-Snary KJ, Snetsinger B, Mewburn JD, Thebaud A, Lima PDA, Thebaud B, Archer SL. The comprehensive transcriptome of human ductus arteriosus smooth muscle cells (hDASMC). *Data Brief*. 2022;40:107736. doi: 10.1016/j.dib.2021.107736
29. Pak O, Nolte A, Knoepp F, Giordano L, Pecina P, Hüttemann M, Grossman LI, Weissmann N, Sommer N. Mitochondrial oxygen sensing of acute hypoxia in specialized cells-Is there a unifying mechanism? *Biochimica et Biophysica Acta (BBA)-Bioenergetics*. 2022;1863:148911.
30. Waypa GB, Marks JD, Guzy RD, Mungai PT, Schriewer JM, Dokic D, Ball MK, Schumacker PT. Superoxide generated at mitochondrial complex III triggers acute responses to hypoxia in the pulmonary circulation. *Am J Respir Crit Care Med*. 2013;187:424-432. doi: 10.1164/rccm.201207-1294OC
31. Sommer N, Huttemann M, Pak O, Scheibe S, Knoepp F, Sinkler C, Malczyk M, Gierhardt M, Esfandiary A, Kraut S, et al. Mitochondrial Complex IV Subunit 4 Isoform 2 Is Essential for Acute Pulmonary Oxygen Sensing. *Circ Res*. 2017;121:424-438. doi: 10.1161/CIRCRESAHA.116.310482
32. Vogel RO, Smeitink JA, Nijtmans LG. Human mitochondrial complex I assembly: a dynamic and versatile process. *Biochimica et Biophysica Acta (BBA)-Bioenergetics*. 2007;1767:1215-1227.
33. Nakamaru-Ogiso E. Iron–sulfur clusters in complex I. *A Structural Perspective on Respiratory Complex I: Structure and Function of NADH: ubiquinone Oxidoreductase*. 2012:61-79.
34. Lambert AJ, Brand MD. Inhibitors of the quinone-binding site allow rapid superoxide production from mitochondrial NADH: ubiquinone oxidoreductase (complex I). *Journal of Biological Chemistry*. 2004;279:39414-39420.

35. Cadenas E, Boveris A, Ragan CI, Stoppani AO. Production of superoxide radicals and hydrogen peroxide by NADH-ubiquinone reductase and ubiquinol-cytochrome c reductase from beef-heart mitochondria. *Archives of biochemistry and biophysics*. 1977;180:248-257.
36. Friedrich T, Hellwig P, Einsle O. On the mechanism of the respiratory complex I. *A Structural Perspective on Respiratory Complex I: Structure and Function of NADH: ubiquinone oxidoreductase*. 2012:23-59.
37. Ni Y, Hagras MA, Konstantopoulou V, Mayr JA, Stuchebrukhov AA, Meierhofer D. Mutations in NDUFS1 cause metabolic reprogramming and disruption of the electron transfer. *Cells*. 2019;8:1149.
38. Read AD, Bentley RE, Archer SL, Dunham-Snary KJ. Mitochondrial iron–sulfur clusters: Structure, function, and an emerging role in vascular biology. *Redox biology*. 2021;47:102164.
39. Orr AL, Ashok D, Sarantos MR, Shi T, Hughes RE, Brand MD. Inhibitors of ROS production by the ubiquinone-binding site of mitochondrial complex I identified by chemical screening. *Free Radical Biology and Medicine*. 2013;65:1047-1059.
40. Orr AL, Vargas L, Turk CN, Baaten JE, Matzen JT, Dardov VJ, Attle SJ, Li J, Quackenbush DC, Goncalves RL. Suppressors of superoxide production from mitochondrial complex III. *Nature chemical biology*. 2015;11:834-836.
41. Čunátová K, Reguera DP, Vrbacký M, Fernández-Vizarra E, Ding S, Fearnley IM, Zeviani M, Houštěk J, Mráček T, Pecina P. Loss of COX4I1 leads to combined respiratory chain deficiency and impaired mitochondrial protein synthesis. *Cells*. 2021;10:369.
42. Cogliati S, Cabrera-Alarcón JL, Enriquez JA. Regulation and functional role of the electron transport chain supercomplexes. *Biochemical Society Transactions*. 2021;49:2655-2668.
43. Schägger H, Pfeiffer K. Supercomplexes in the respiratory chains of yeast and mammalian mitochondria. *The EMBO journal*. 2000.
44. Acín-Pérez R, Bayona-Bafaluy MaP, Fernández-Silva P, Moreno-Loshuertos R, Pérez-Martos A, Bruno C, Moraes CT, Enríquez JA. Respiratory complex III is required to maintain complex I in mammalian mitochondria. *Molecular cell*. 2004;13:805-815.
45. Schägger H, de Coo R, Bauer MF, Hofmann S, Godinot C, Brandt U. Significance of respirasomes for the assembly/stability of human respiratory chain complex I. *Journal of Biological Chemistry*. 2004;279:36349-36353.
46. Protasoni M, Pérez-Pérez R, Lobo-Jarne T, Harbour ME, Ding S, Peñas A, Diaz F, Moraes CT, Fearnley IM, Zeviani M. Respiratory supercomplexes act as a platform for complex III-mediated maturation of human mitochondrial complexes I and IV. *The EMBO journal*. 2020;39:e102817.
47. Diaz F, Fukui H, Garcia S, Moraes CT. Cytochrome c oxidase is required for the assembly/stability of respiratory complex I in mouse fibroblasts. *Molecular and cellular biology*. 2006;26:4872-4881.
48. Douiev L, Miller C, Ruppo S, Benyamini H, Abu-Libdeh B, Saada A. Upregulation of COX4-2 via HIF-1α in Mitochondrial COX4-1 Deficiency. *Cells*. 2021;10:452.
49. Bieging-Rolett KT, Kaiser AM, Morgens DW, Boutelle AM, Seoane JA, Van Nostrand EL, Zhu C, Houlihan SL, Mello SS, Yee BA. Zmat3 is a key splicing regulator in the p53 tumor suppression program. *Molecular cell*. 2020;80:452-469. e459.
50. Shi H-Y, Xie M-S, Yang C-X, Huang R-T, Xue S, Liu X-Y, Xu Y-J, Yang Y-Q. Identification of SOX18 as a new gene predisposing to congenital heart disease. *Diagnostics*. 2022;12:1917.
51. Muys BR, Shrestha RL, Anastasakis DG, Pongor L, Li XL, Grammatikakis I, Polash A, Chari R, Gorospe M, Harris CC. Matrin3 regulates mitotic spindle dynamics by controlling alternative splicing of CDC14B. *Cell reports*. 2023;42.
52. Quintero-Rivera F, Xi QJ, Keppler-Noreuil KM, Lee JH, Higgins AW, Anchan RM, Roberts AE, Seong IS, Fan X, Lage K. MATR3 disruption in human and mouse associated with bicuspid aortic valve, aortic coarctation and patent ductus arteriosus. *Human molecular genetics*. 2015;24:2375-2389.

53. Böhlig L, Metzger R, Rother K, Till H, Engeland K. The CCN3 gene coding for an extracellular adhesion-related protein is transcriptionally activated by the p53 tumor suppressor. *Cell Cycle*. 2008;7:1254-1261.
54. Iwai K, Nagasawa K, Akaike T, Oshima T, Kato T, Minamisawa S. CCN3 secreted by prostaglandin E2 inhibits intimal cushion formation in the rat ductus arteriosus. *Biochemical and biophysical research communications*. 2018;503:3242-3247.
55. Zhou S, Cai Y, Xu Z, Peng B, Liang Q, Peng J, Yan Y. Identification of a pyroptosis-related lncRNA signature in the regulation of prognosis, metabolism signals and immune infiltration in lung adenocarcinoma. *Frontiers in Endocrinology*. 2022;13:964362.
56. Wang Y, Wang X, Xu Q, Yin J, Wang H, Zhang L. CircRNA, lncRNA, and mRNA profiles of umbilical cord blood exosomes from preterm newborns showing bronchopulmonary dysplasia. *European journal of pediatrics*. 2022;181:3345-3365.
57. Yang Q, Fan W, Lai B, Liao B, Deng M. lncRNA-TCONS_00008552 expression in patients with pulmonary arterial hypertension due to congenital heart disease. *Plos one*. 2023;18:e0281061.
58. Gehart H, Goginashvili A, Beck R, Morvan J, Erbs E, Formentini I, De Matteis MA, Schwab Y, Wieland FT, Ricci R. The BAR domain protein Arfaptin-1 controls secretory granule biogenesis at the trans-Golgi network. *Developmental cell*. 2012;23:756-768.
59. Judith D, Jefferies HB, Boeing S, Frith D, Snijders AP, Tooze SA. ATG9A shapes the forming autophagosome through Arfaptin 2 and phosphatidylinositol 4-kinase IIIβ. *Journal of Cell Biology*. 2019;218:1634-1652.
60. Zhou L, Ouyang L, Chen K, Wang X. Research progress on KIF3B and related diseases. *Annals of translational medicine*. 2019;7.
61. Malumbres M. Cyclin-dependent kinases. *Genome biology*. 2014;15:1-10.
62. Karimbayli J, Pellarin I, Belletti B, Baldassarre G. Insights into the structural and functional activities of forgotten Kinases: PCTAIREs CDKs. *Molecular Cancer*. 2024;23:135.
63. Ye L, Yu Y, Zhao Z-A, Zhao D, Ni X, Wang Y, Fang X, Yu M, Wang Y, Tang J-M. Patient-specific iPSC-derived cardiomyocytes reveal abnormal regulation of FGF16 in a familial atrial septal defect. *Cardiovascular research*. 2022;118:859-871.
64. Botero V, Garcia VH, Gomez-Duarte C, Aristizabal AM, Arrunategui AM, Echeverri GJ, Pachajoa H. Lysosomal acid lipase deficiency, a rare pathology: the first pediatric patient reported in Colombia. *The American Journal of Case Reports*. 2018;19:669.
65. Dagle JM, Lepp NT, Cooper ME, Schaa KL, Kelsey KJ, Orr KL, Caprau D, Zimmerman CR, Steffen KM, Johnson KJ. Determination of genetic predisposition to patent ductus arteriosus in preterm infants. *Pediatrics*. 2009;123:1116-1123.
66. Yarboro MT, Durbin MD, Herington JL, Shelton EL, Zhang T, Ebby CG, Stoller JZ, Clyman RI, Reese J. Transcriptional profiling of the ductus arteriosus: Comparison of rodent microarrays and human RNA sequencing. *Semin Perinatol*. 2018;42:212-220. doi: 10.1053/j.semperi.2018.05.003
67. Lewis TR, Shelton EL, Van Driest SL, Kannankeril PJ, Reese J. Genetics of the patent ductus arteriosus (PDA) and pharmacogenetics of PDA treatment. Paper/Poster presented at: Seminars in Fetal and Neonatal Medicine; 2018;
68. Ndour D, Bouamari H, Berthiller J, Claris O, Plaisant F, Nguyen K. Adverse events related to ibuprofen treatment for patent ductus arteriosus in premature neonates. *Archives de Pédiatrie*. 2020;27:452-455.

## 7. Figure Legends

### Figure 1: Ductus Arteriosus Smooth Muscle Cell Oxygen Sensing and Experimental Design

**A**) The fetal (left) hypoxic arterial partial pressure of oxygen ($pO_2$, ~40 mmHg) maintains a patent ductus arteriosus (DA), diverting placentally oxygenated blood to the aorta. The neonatal (right) rise in $pO_2$ (70-100 mmHg) causes DA constriction. **B**) In DA smooth muscle cell (DASMC), in hypoxia (left), there is low mitochondrial generation of reactive oxygen species (ROS), maintaining a polarized resting membrane potential ($E_M$) and low concentrations of intracellular calcium $[Ca^{2+}]_i$ (voltage-gated potassium channels = purple, L-type calcium channels = blue). Under normoxic conditions (right), increased mitochondrial ROS generation promotes influx of calcium and activation of myosin to increase DASMC tension. The mitochondrial-targeted antioxidant, MitoTEMPO, and knockdown of NDUFS2 (siNDUFS2) both inhibit the increase in ROS. **C**) To examine the importance of putative mitochondrial $O_2$-sensor proteins we selectively knocked down **Complex I subunits: 1**) NADH:Ubiquinone oxidoreductase core subunit S1 (NDUFS1), located near the NADH binding site. **2**) NADH:Ubiquinone oxidoreductase core subunit S2 (NDUFS2), at the ubiquinone binding site. **3**) NADH:Ubiquionone oxidoreductase core subunit S7 (NDUFS7), also at the ubiquinone binding site. **Complex III subunit: 4**) Ubiquinol-cytochrome c reductase, Rieske iron-sulfur polypeptide 1 (UQCRFS1), at the Rieske iron-sulfur cluster. **Complex IV subunit: 5**) Cytochrome c oxidase subunit 4I2 (COX4I2).
Created in BioRender. Bentley, R. (2025) https://BioRender.com/o096p30

### Figure 2: Confirmation of ETC Subunit Knockdown at the mRNA and Protein Level

**A-C**) NDUFS1 mRNA (n=4 cell lines) and protein (n=7 cell lines) were significantly reduced following siNDUFS1 versus siControl. **D-F**) siNDUFS2 significantly decreased expression of NDUFS2 mRNA (n=6 cell lines) and protein (n=7 cell lines) versus siControl. **G-I**) siNDUFS7 significantly decreased expression of NDUFS7 mRNA (n=6 cell lines) and protein (n=6 cell lines) versus siControl. **J-L**) siUQCRFS1 significantly decreased expression of UQCRFS1 mRNA (n=6 cell lines) and protein (n=7 cell lines) versus siControl. **M-O**) siCOX4I2 significantly decreased expression of COX4I2 mRNA (n=3 cell lines) and protein (n=5 cell lines).
All measurements made 48-hours post siRNA treatment. Three technical replicates were run for qRT-PCRs. For all immunoblots, representative gels shown and expression normalized to beta-actin.

### Figure 3: NDUFS2 Mediates ROS Production and Vasoconstriction in Response to Oxygen in human DASMC

Oxygen responsiveness was assessed using live confocal imaging with the calcium sensitive dye Cal-520AM. (**A**) Representative images of DASMC measured after 20-minutes in hypoxia (left, 3.5% oxygen), 20-minutes normoxia (middle, 19% oxygen), and with the addition of 80mM KCl (right) as a positive control. Cells lacking a KCl-induced rise in intracellular calcium were excluded from analysis. **B**) Treatment with siControl caused no change in normoxia-induced rise in $[Ca^{2+}]_i$ versus untreated cells, whereas siNDUFS2 significantly reduced the oxygen-induced increase in $[Ca^{2+}]_i$ (n=10 cell lines, 10-20 cells/cell line). **C**) There was also no effect of siControl on DASMC constriction compared to untreated cells, measured as % cell shortening versus hypoxic baseline, whereas siNDUFS2 significantly decrease normoxia-induced constriction (n=10 cell lines, 10 cells/cell line). **D**) Representative images showing mROS measured using MitoROS™ 580 in hypoxia (3% oxygen) and normoxia (19% oxygen) in untreated cells (left and middle-left), with antioxidant (MitoTEMPO, middle-right), and following NDUFS2 knockdown (right). **E**) In untreated cells, there was a significant rise in mROS generation in normoxia, with a significant decrease in normoxic mROS generation with MitoTEMPO and siNDUFS2 (n=4 cell lines, 10 cells/cell line). **F**) MitoTEMPO significantly decreased oxygen-induced cell shortening, to a similar degree as NDUFS2 knockdown (n=4 cell lines, 10 cells/cell line).

**Figure 4: Selective Knockdown of ETC Subunits Does Not Inhibit Mitochondrial Subunit Function**

**A**) Complex I activity was measured using a dipstick assay of hDASMC treated for 48h with siRNA targeting control, NDUFS2, NDUFS1, NDUFS7, UQCRFS1, and COX4I2. **B**) Complex I activity was only significantly reduced by treatment with siNDUFS1 (n=8 cell lines). **C**) Complex III activity, normalized to µg of protein, was not significantly changed by treatment of any siRNA including siUQCRFS1 (n=5 cell lines). **D**) There was no significant difference in Complex IV activity with 48h treatment with any siRNA treatment, including siCOX4I2 (n=8 cell lines).

**Figure 5: Selective Knockdown of ETC Subunits Does Not Inhibit Mitochondrial Respiration**

**A**) A Seahorse XF mitochondrial stress test measured oxygen consumption rate (OCR) of hDASMC treated for 48-hours with siRNA targeting control (NC) or ETC subunits: NDUFS2, NDUFS1, NDUFS7, UQCRFS1, or COX4I2. Knockdown of ETC subunits (n=5 cell lines, 3 technical replicates) caused no change in key measures of mitochondrial respiration, including (**B**) basal respiration, (**C**) spare respiratory capacity, or (**D**) ATP-linked respiration. OCR in each cell line and treatment was normalized to total µg protein.

**Figure 6: Transcriptomics Reveal Unique Downstream Effects of Selective Knockdown of ETC Subunits on Gene Expression**

**A**) There were numerous differentially expressed genes (DEGs) significantly regulated by each knockdown condition compared to siControl, with 677 common DEGs across all knockdown conditions. **B**) Heat map of the top 20 siNDUFS2 versus siControl DEGs with each siRNA, reveals both unique (highlighted in green) and common regulation of genes amongst knockdown conditions. Colour was scaled by fold change achieved by each knockdown versus siControl.

**Figure 7: Gene Ontology (GO) Enrichment Analysis of Differentially Expressed Genes (DEGs) Uniquely Regulated by NDUFS2 Knockdown Reveals Key Mitochondrial Pathways**

The top 20 significantly enriched (adjusted $p<0.05$) GO terms in the (**A**) Biological Process, (**B**) Cellular Component, and **(C**) Molecular Function domains, ranked by the number of genes involved in each GO term (count). Mitochondrially related pathways are indicated by an asterisk (*).

**Figure 8: Mitochondrial Gene Ontology (GO) Pathways with NDUFS2 Knockdown**

Significantly enriched GO terms with NDUFS2 knockdown versus siControl were filtered by the search string “mitoc” to explore the mitochondrial pathways affected by siNDUFS2. Sorting by adjusted p-value, the first appearing mitochondrial term, “mitochondrial inner membrane” (GO:0005743), is the second of 101 significantly enriched GO terms for the 578 genes uniquely DE between siNDUFS2 and siControl.

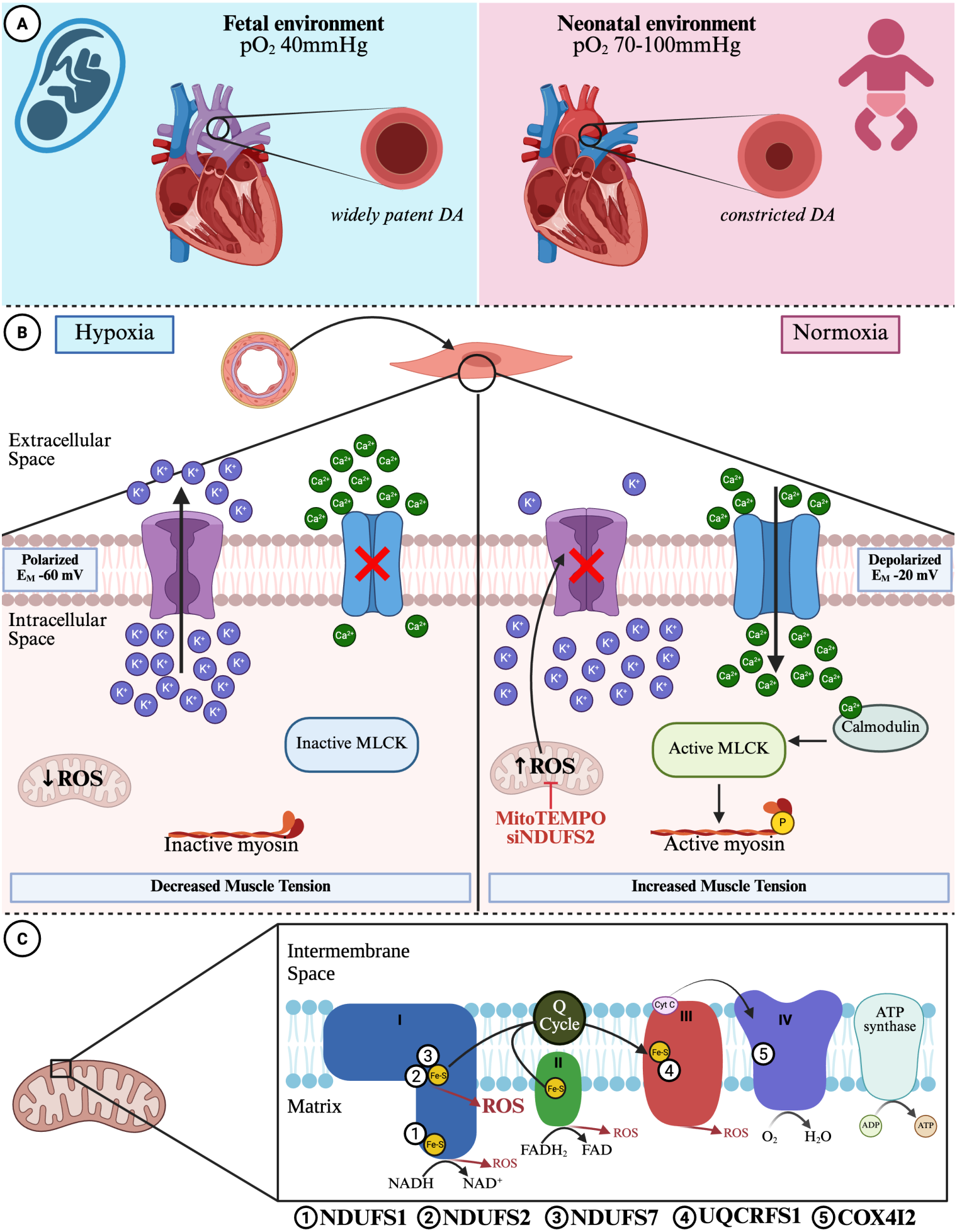
A
Fetal environment
pO2 40mmHg
widely patent DA
Neonatal environment
pO2 70-100mmHg
constricted DA
B
Hypoxia
Normoxia
Extracellular Space
Intracellular Space
Polarized EM -60 mV
Depolarized EM -20 mV
Inactive MLCK
↓ROS
Inactive myosin
Decreased Muscle Tension
↑ROS
MitoTEMPO
siNDUFS2
Calmodulin
Active MLCK
Active myosin
Increased Muscle Tension
C
Intermembrane Space
Matrix
Q Cycle
Cyt C
ATP synthase
ROS
NADH
NAD+
FADH2
FAD
O2
H2O
ADP
ATP
①NDUFS1 ②NDUFS2 ③NDUFS7 ④UQCRFS1 ⑤COX4I2

**Figure 1: Ductus Arteriosus Smooth Muscle Cell Oxygen Sensing and Experimental Design**

**A**) The fetal (left) hypoxic arterial partial pressure of oxygen ($pO_2$, ~40 mmHg) maintains a patent ductus arteriosus (DA), diverting placentally oxygenated blood to the aorta. The neonatal (right) rise in $pO_2$ (70-100 mmHg) causes DA constriction. **B**) In DA smooth muscle cell (DASMC), in hypoxia (left), there is low mitochondrial generation of reactive oxygen species (ROS), maintaining a polarized resting membrane potential ($E_M$) and low concentrations of intracellular calcium $[Ca^{2+}]_i$ (voltage-gated potassium channels = purple, L-type calcium channels = blue). Under normoxic conditions (right), increased mitochondrial ROS generation promotes influx of calcium and activation of myosin to increase DASMC tension. The mitochondrial-targeted antioxidant, MitoTEMPO, and knockdown of NDUFS2 (siNDUFS2) both inhibit the increase in ROS. **C**) To examine the importance of putative mitochondrial $O_2$-sensor proteins we selectively knocked down **Complex I subunits: 1**) NADH:Ubiquinone oxidoreductase core subunit S1 (NDUFS1), located near the NADH binding site. **2**) NADH:Ubiquinone oxidoreductase core subunit S2 (NDUFS2), at the ubiquinone binding site. **3**) NADH:Ubiquionone oxidoreductase core subunit S7 (NDUFS7), also at the ubiquinone binding site. **Complex III subunit: 4**) Ubiquinol-cytochrome c reductase, Rieske iron-sulfur polypeptide 1 (UQCRFS1), at the Rieske iron-sulfur cluster. **Complex IV subunit: 5**) Cytochrome c oxidase subunit 4I2 (COX4I2).
Created in BioRender. Bentley, R. (2025) https://BioRender.com/o096p30

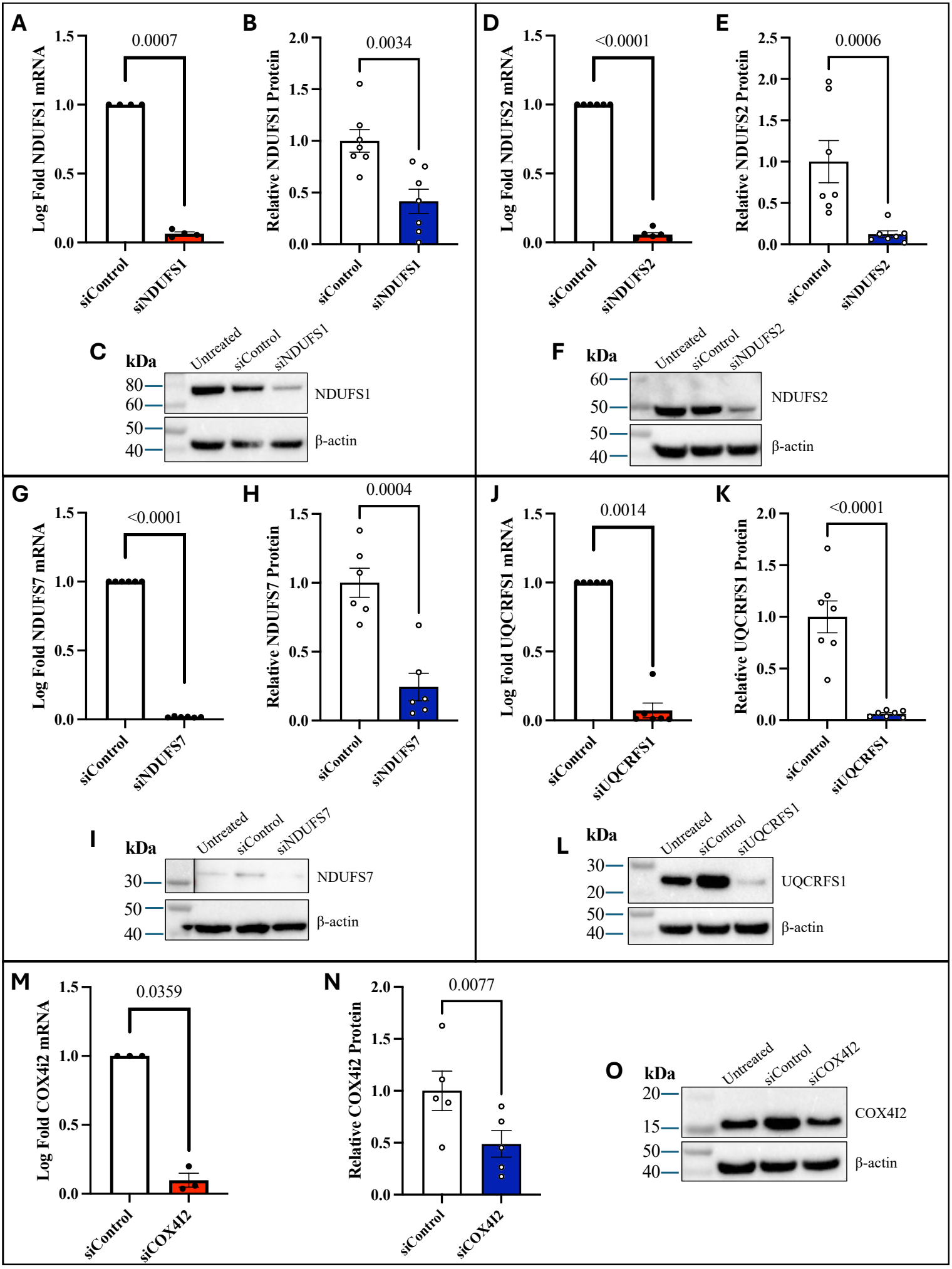
A
Log Fold NDUFS1 mRNA
0.0007
siControl
siNDUFS1
B
Relative NDUFS1 Protein
0.0034
C
kDa
Untreated
siControl
siNDUFS1
NDUFS1
β-actin
D
Log Fold NDUFS2 mRNA
<0.0001
siNDUFS2
E
Relative NDUFS2 Protein
0.0006
F
NDUFS2
G
Log Fold NDUFS7 mRNA
<0.0001
siNDUFS7
H
Relative NDUFS7 Protein
0.0004
I
NDUFS7
J
Log Fold UQCRFS1 mRNA
0.0014
siUQCRFS1
K
Relative UQCRFS1 Protein
<0.0001
L
UQCRFS1
M
Log Fold COX4i2 mRNA
0.0359
siCOX4I2
N
Relative COX4I2 Protein
0.0077
O
COX4I2

**Figure 2: Confirmation of ETC Subunit Knockdown at the mRNA and Protein Level**

**A-C**) NDUFS1 mRNA (n=4 cell lines) and protein (n=7 cell lines) were significantly reduced following siNDUFS1 versus siControl. **D-F**) siNDUFS2 significantly decreased expression of NDUFS2 mRNA (n=6 cell lines) and protein (n=7 cell lines) versus siControl. **G-I**) siNDUFS7 significantly decreased expression of NDUFS7 mRNA (n=6 cell lines) and protein (n=6 cell lines) versus siControl. **J-L**) siUQCRFS1 significantly decreased expression of UQCRFS1 mRNA (n=6 cell lines) and protein (n=7 cell lines) versus siControl. **M-O**) siCOX4I2 significantly decreased expression of COX4I2 mRNA (n=3 cell lines) and protein (n=5 cell lines).

All measurements made 48-hours post siRNA treatment. Three technical replicates were run for qRT-PCRs. For all immunoblots, representative gels shown and expression normalized to beta-actin.

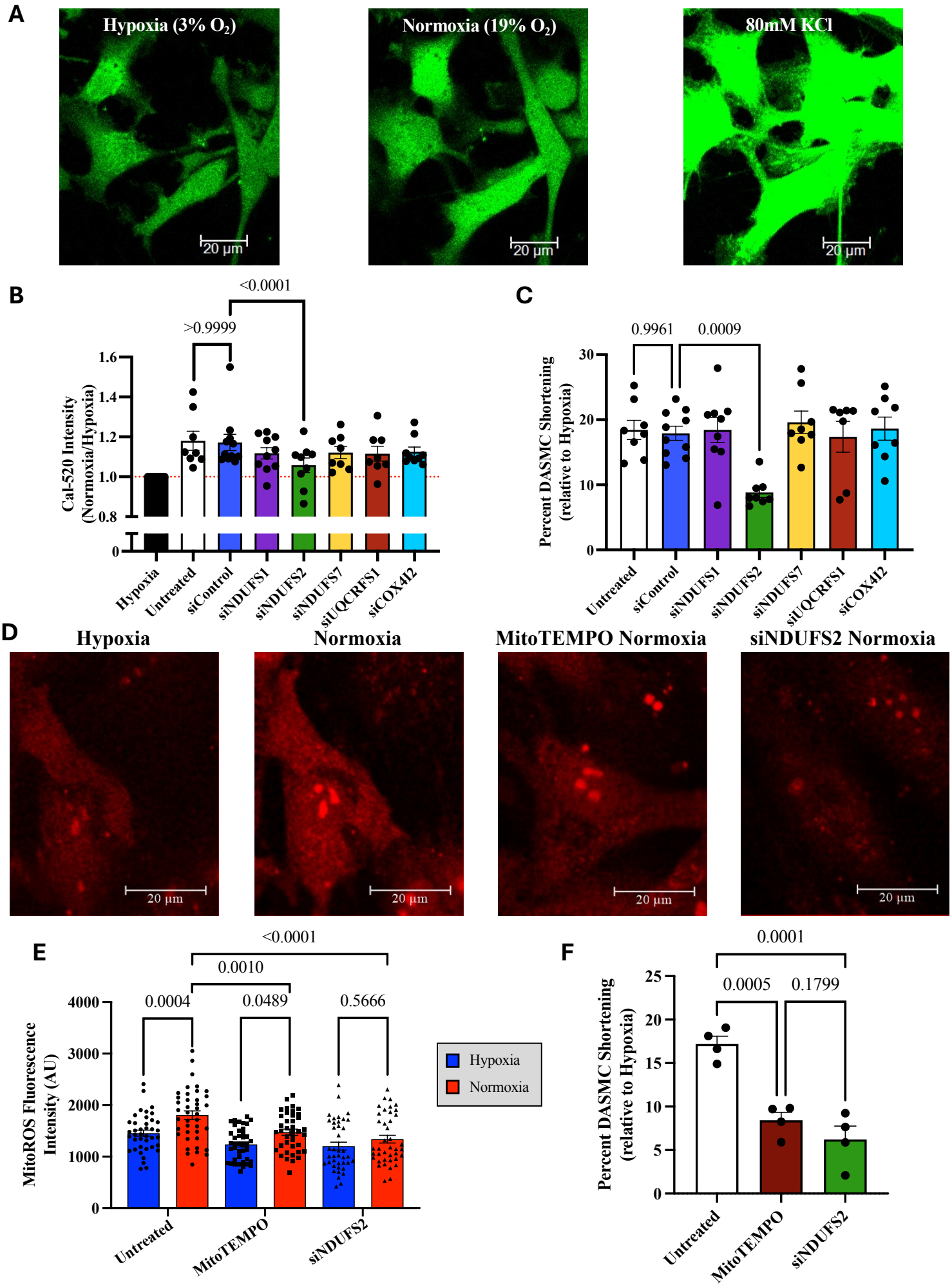
A
Hypoxia (3% O2)
Normoxia (19% O2)
80mM KCl
20 µm
B
<0.0001
>0.9999
Cal-520 Intensity (Normoxia/Hypoxia)
1.6
1.4
1.2
1.0
0.8
0
Hypoxia
Untreated
siControl
siNDUFS1
siNDUFS2
siNDUFS7
siUQCRFS1
siCOX4I2
C
0.9961
0.0009
Percent DASMC Shortening (relative to Hypoxia)
30
20
10
0
Untreated
siControl
siNDUFS1
siNDUFS2
siNDUFS7
siUQCRFS1
siCOX4I2
D
Hypoxia
Normoxia
MitoTEMPO Normoxia
siNDUFS2 Normoxia
20 µm
E
<0.0001
0.0010
0.0004
0.0489
0.5666
MitoROS Fluorescence Intensity (AU)
4000
3000
2000
1000
0
Untreated
MitoTEMPO
siNDUFS2
Hypoxia
Normoxia
F
0.0001
0.0005
0.1799
Percent DASMC Shortening (relative to Hypoxia)
25
20
15
10
5
0
Untreated
MitoTEMPO
siNDUFS2

**Figure 3: NDUFS2 Mediates ROS Production and Vasoconstriction in Response to Oxygen in human DASMC**

Oxygen responsiveness was assessed using live confocal imaging with the calcium sensitive dye Cal-520AM. (**A**) Representative images of DASMC measured after 20-minutes in hypoxia (left, 3.5% oxygen), 20-minutes normoxia (middle, 19% oxygen), and with the addition of 80mM KCl (right) as a positive control. Cells lacking a KCl-induced rise in intracellular calcium were excluded from analysis. **B**) Treatment with siControl caused no change in normoxia-induced rise in $[Ca^{2+}]_i$ versus untreated cells, whereas siNDUFS2 significantly reduced the oxygen-induced increase in $[Ca^{2+}]_i$ (n=10 cell lines, 10-20 cells/cell line). **C**) There was also no effect of siControl on DASMC constriction compared to untreated cells, measured as % cell shortening versus hypoxic baseline, whereas siNDUFS2 significantly decrease normoxia-induced constriction (n=10 cell lines, 10 cells/cell line). **D**) Representative images showing mROS measured using MitoROS™ 580 in hypoxia (3% oxygen) and normoxia (19% oxygen) in untreated cells (left and middle-left), with antioxidant (MitoTEMPO, middle-right), and following NDUFS2 knockdown (right). **E**) In untreated cells, there was a significant rise in mROS generation in normoxia, with a significant decrease in normoxic mROS generation with MitoTEMPO and siNDUFS2 (n=4 cell lines, 10 cells/cell line). **F**) MitoTEMPO significantly decreased oxygen-induced cell shortening, to a similar degree as NDUFS2 knockdown (n=4 cell lines, 10 cells/cell line).

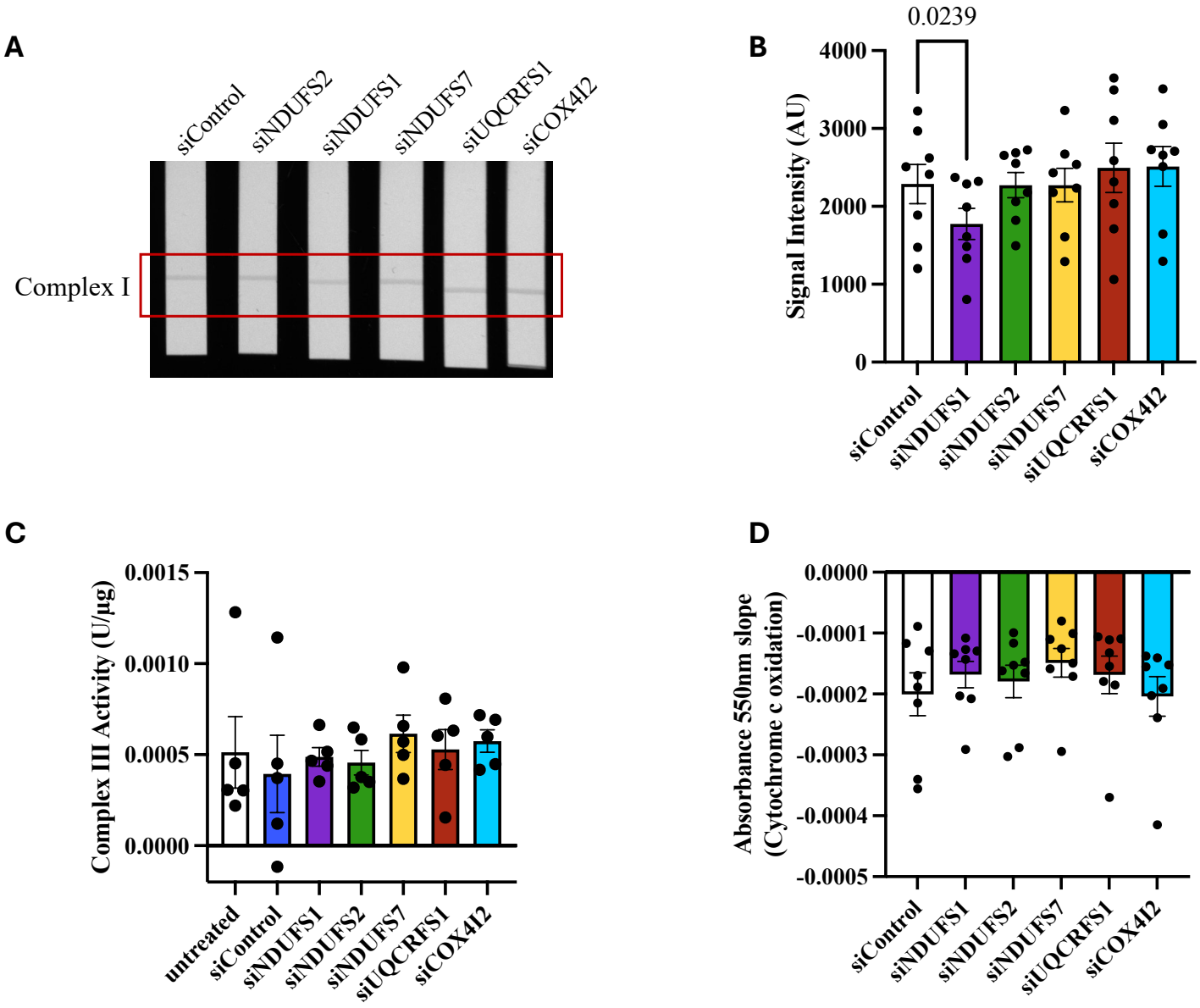


**Figure 4: Selective Knockdown of ETC Subunits Does Not Inhibit Mitochondrial Subunit Function**

**A**) Complex I activity was measured using a dipstick assay of hDASMC treated for 48h with siRNA targeting control, NDUFS2, NDUFS1, NDUFS7, UQCRFS1, and COX4I2. **B**) Complex I activity was only significantly reduced by treatment with siNDUFS1 (n=8 cell lines). **C**) Complex III activity, normalized to µg of protein, was not significantly changed by treatment of any siRNA including siUQCRFS1 (n=5 cell lines). **D**) There was no significant difference in Complex IV activity with 48h treatment with any siRNA treatment, including siCOX4I2 (n=8 cell lines).

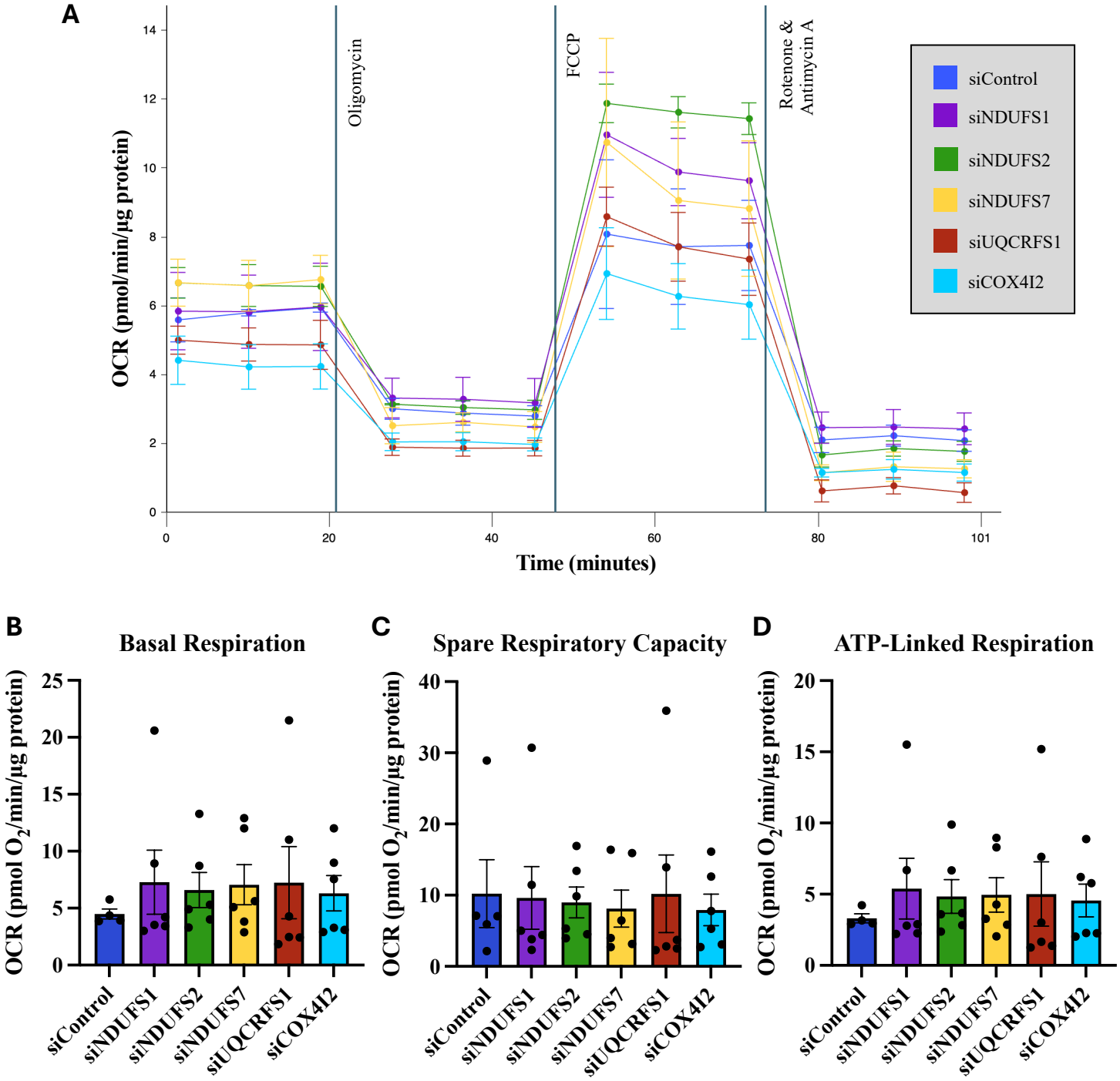


**Figure 5: Selective Knockdown of ETC Subunits Does Not Inhibit Mitochondrial Respiration**

**A**) A Seahorse XF mitochondrial stress test measured oxygen consumption rate (OCR) of hDASMC treated for 48-hours with siRNA targeting control (NC) or ETC subunits: NDUFS2, NDUFS1, NDUFS7, UQCRFS1, or COX4I2. Knockdown of ETC subunits (n=5 cell lines, 3 technical replicates) caused no change in key measures of mitochondrial respiration, including (**B**) basal respiration, (**C**) spare respiratory capacity, or (**D**) ATP-linked respiration. OCR in each cell line and treatment was normalized to total µg protein.

A

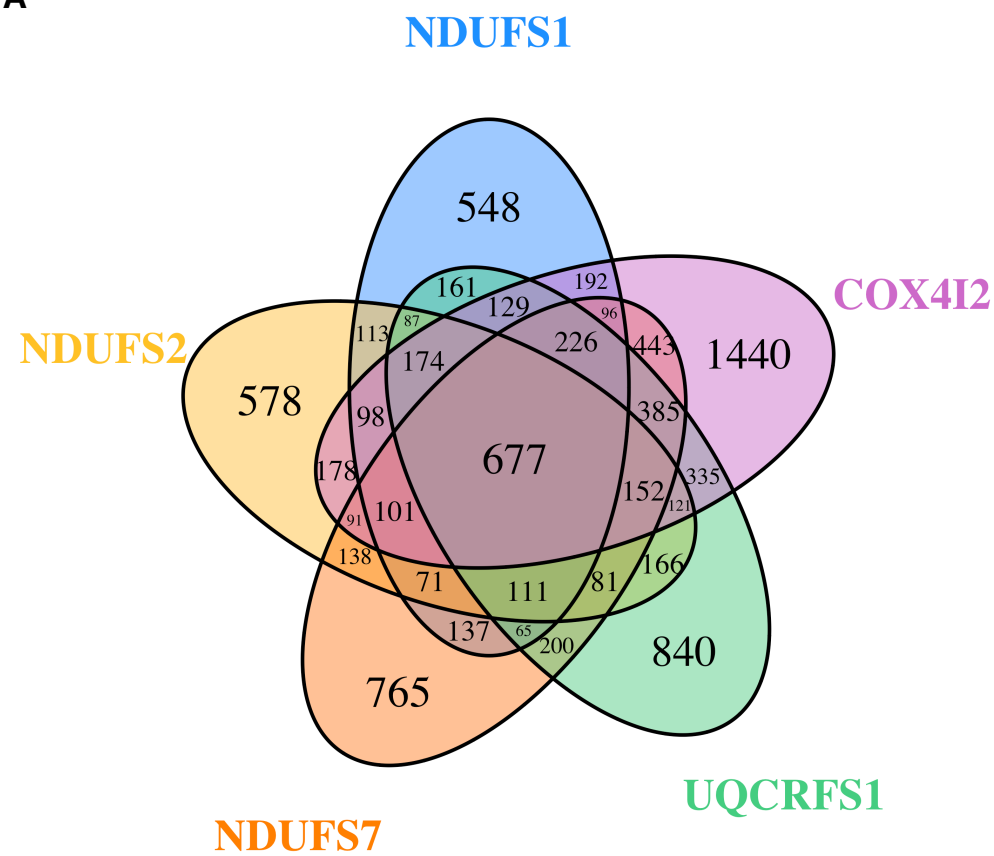
NDUFS1
548
161
129
192
96
COX4I2
1440
443
226
NDUFS2
578
113
87
174
98
385
677
178
335
152
121
101
91
138
71
111
81
166
137
65
200
840
765
UQCRFS1
NDUFS7

B

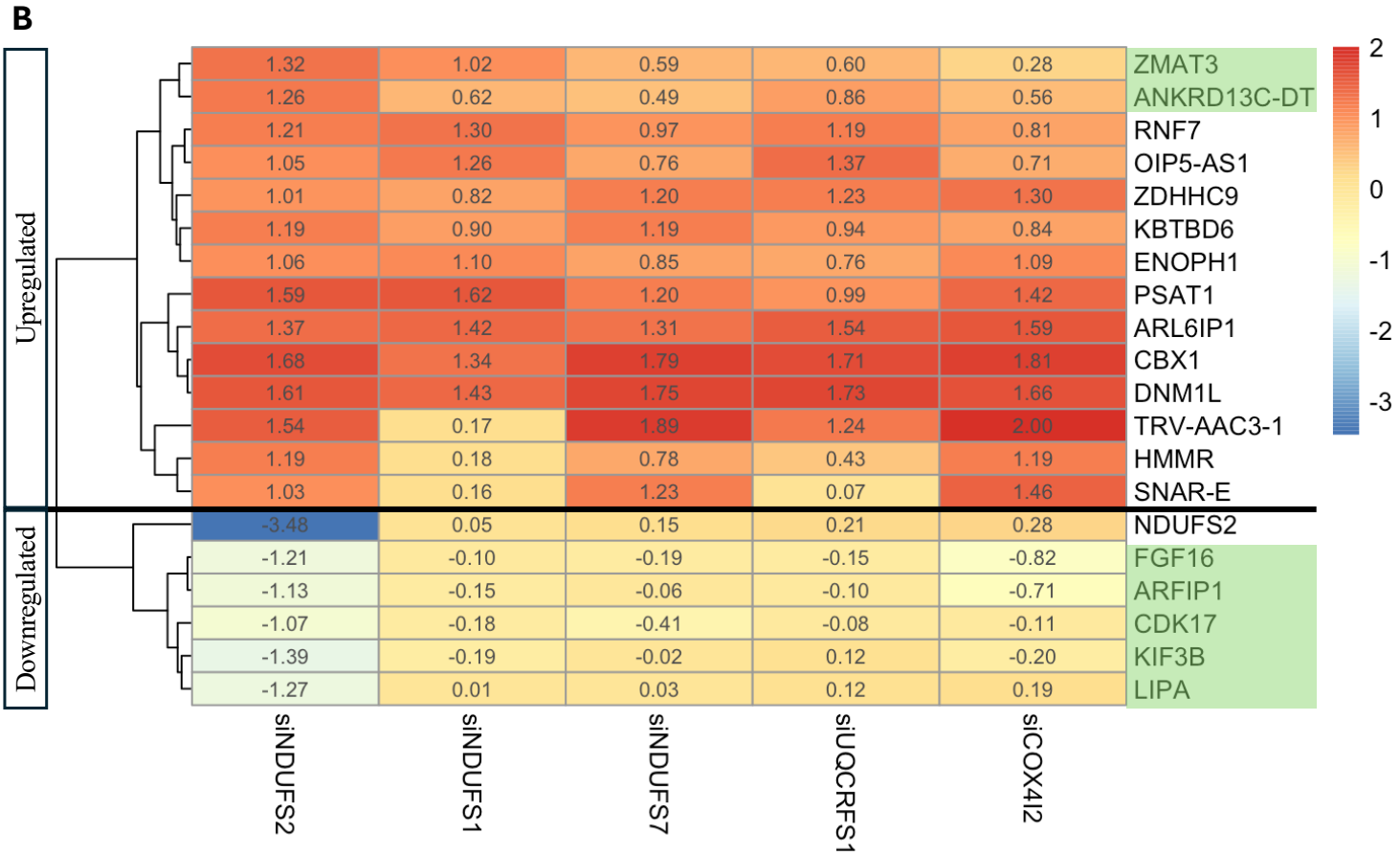
Upregulated
Downregulated
1.32 1.02 0.59 0.60 0.28 ZMAT3
1.26 0.62 0.49 0.86 0.56 ANKRD13C-DT
1.21 1.30 0.97 1.19 0.81 RNF7
1.05 1.26 0.76 1.37 0.71 OIP5-AS1
1.01 0.82 1.20 1.23 1.30 ZDHHC9
1.19 0.90 1.19 0.94 0.84 KBTBD6
1.06 1.10 0.85 0.76 1.09 ENOPH1
1.59 1.62 1.20 0.99 1.42 PSAT1
1.37 1.42 1.31 1.54 1.59 ARL6IP1
1.68 1.34 1.79 1.71 1.81 CBX1
1.61 1.43 1.75 1.73 1.66 DNM1L
1.54 0.17 1.89 1.24 2.00 TRV-AAC3-1
1.19 0.18 0.78 0.43 1.19 HMMR
1.03 0.16 1.23 0.07 1.46 SNAR-E
-3.48 0.05 0.15 0.21 0.28 NDUFS2
-1.21 -0.10 -0.19 -0.15 -0.82 FGF16
-1.13 -0.15 -0.06 -0.10 -0.71 ARFIP1
-1.07 -0.18 -0.41 -0.08 -0.11 CDK17
-1.39 -0.19 -0.02 0.12 -0.20 KIF3B
-1.27 0.01 0.03 0.12 0.19 LIPA
siNDUFS2
siNDUFS1
siNDUFS7
siUQCRFS1
siCOX4I2
2
1
0
-1
-2
-3

**Figure 6: Transcriptomics Reveal Unique Downstream Effects of Selective Knockdown of ETC Subunits on Gene Expression**

**A**) There were numerous differentially expressed genes (DEGs) significantly regulated by each knockdown condition compared to siControl, with 677 common DEGs across all knockdown conditions. **B**) Heat map of the top 20 siNDUFS2 versus siControl DEGs with each siRNA, reveals both unique (highlighted in green) and common regulation of genes amongst knockdown conditions. Colour was scaled by fold change achieved by each knockdown versus siControl.

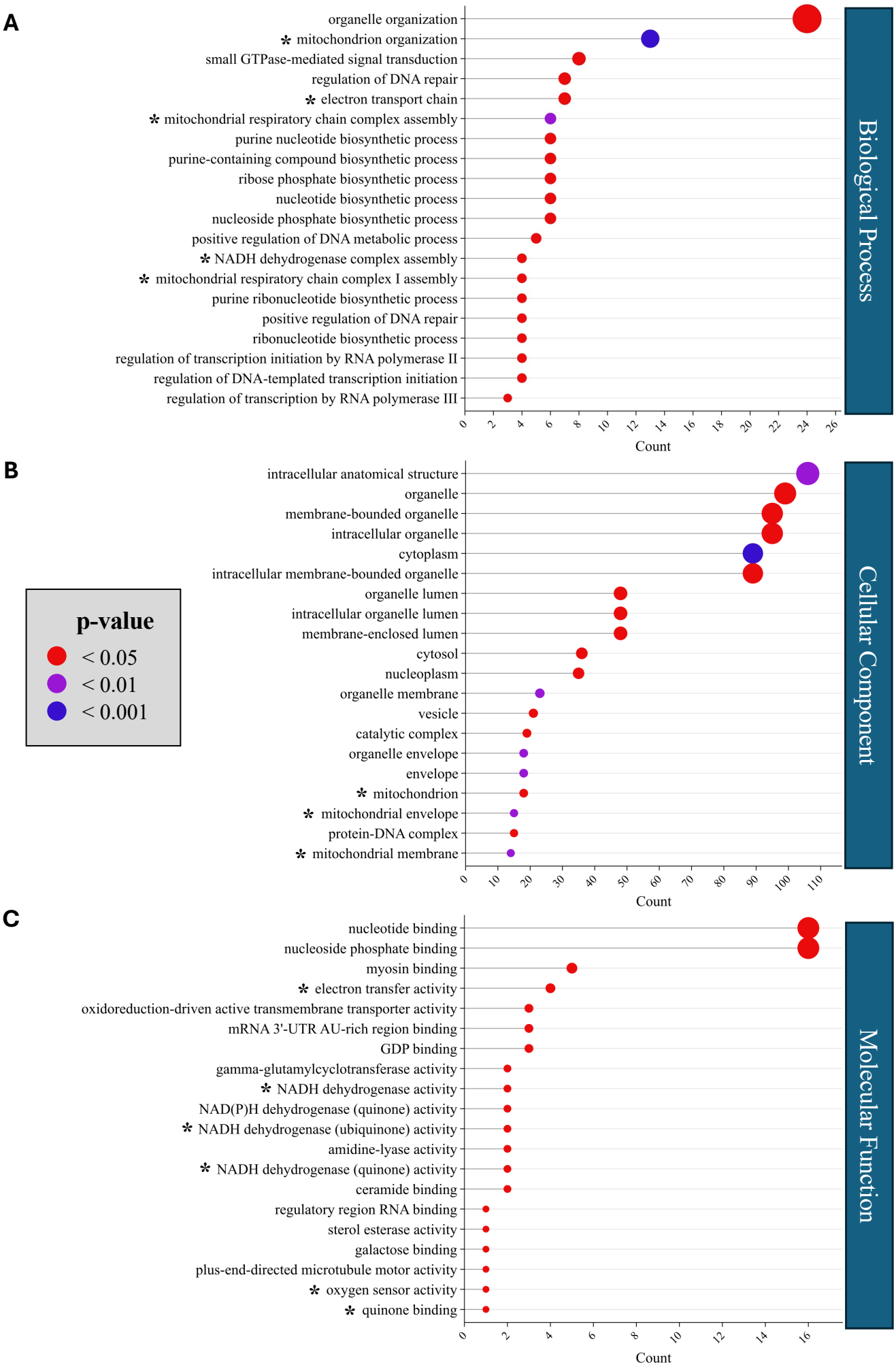
A
organelle organization
* mitochondrion organization
small GTPase-mediated signal transduction
regulation of DNA repair
* electron transport chain
* mitochondrial respiratory chain complex assembly
purine nucleotide biosynthetic process
purine-containing compound biosynthetic process
ribose phosphate biosynthetic process
nucleotide biosynthetic process
nucleoside phosphate biosynthetic process
positive regulation of DNA metabolic process
* NADH dehydrogenase complex assembly
* mitochondrial respiratory chain complex I assembly
purine ribonucleotide biosynthetic process
positive regulation of DNA repair
ribonucleotide biosynthetic process
regulation of transcription initiation by RNA polymerase II
regulation of DNA-templated transcription initiation
regulation of transcription by RNA polymerase III
0 2 4 6 8 10 12 14 16 18 20 22 24 26
Count
Biological Process
B
intracellular anatomical structure
organelle
membrane-bounded organelle
intracellular organelle
cytoplasm
intracellular membrane-bounded organelle
organelle lumen
intracellular organelle lumen
membrane-enclosed lumen
cytosol
nucleoplasm
organelle membrane
vesicle
catalytic complex
organelle envelope
envelope
* mitochondrion
* mitochondrial envelope
protein-DNA complex
* mitochondrial membrane
0 10 20 30 40 50 60 70 80 90 100 110
Count
Cellular Component
p-value
< 0.05
< 0.01
< 0.001
C
nucleotide binding
nucleoside phosphate binding
myosin binding
* electron transfer activity
oxidoreduction-driven active transmembrane transporter activity
mRNA 3'-UTR AU-rich region binding
GDP binding
gamma-glutamylcyclotransferase activity
* NADH dehydrogenase activity
NAD(P)H dehydrogenase (quinone) activity
* NADH dehydrogenase (ubiquinone) activity
amidine-lyase activity
* NADH dehydrogenase (quinone) activity
ceramide binding
regulatory region RNA binding
sterol esterase activity
galactose binding
plus-end-directed microtubule motor activity
* oxygen sensor activity
* quinone binding
0 2 4 6 8 10 12 14 16
Count
Molecular Function

**Figure 7: Gene Ontology (GO) Enrichment Analysis of Differentially Expressed Genes (DEGs) Uniquely Regulated by NDUFS2 Knockdown Reveals Key Mitochondrial Pathways**

The top 20 significantly enriched (adjusted $p<0.05$) GO terms in the (**A**) Biological Process, (**B**) Cellular Component, and **(C**) Molecular Function domains, ranked by the number of genes involved in each GO term (count). Mitochondrially related pathways are indicated by an asterisk (*).

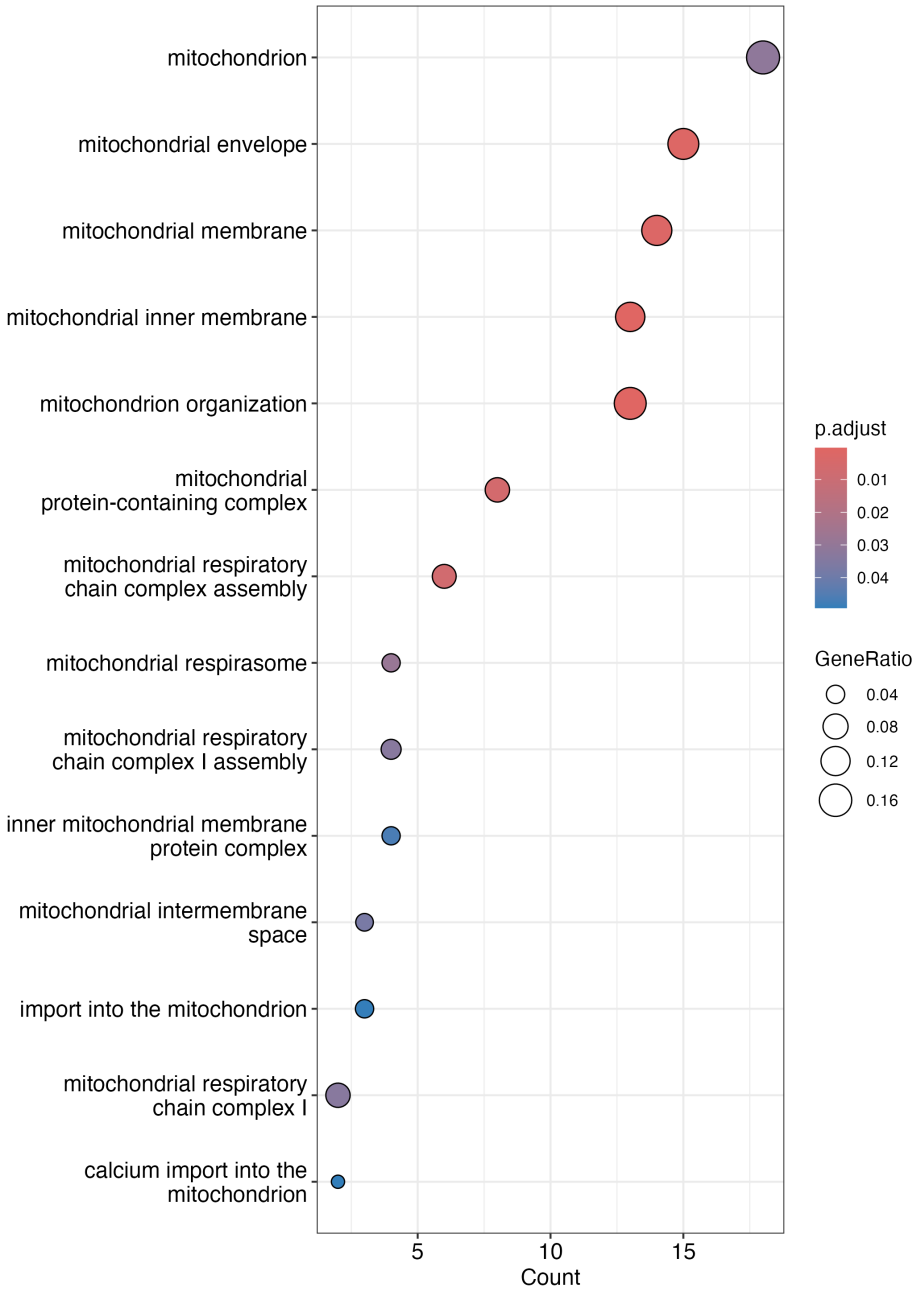


**Figure 8: Mitochondrial Gene Ontology (GO) Pathways with NDUFS2 Knockdown**

Significantly enriched GO terms with NDUFS2 knockdown versus siControl were filtered by the search string "mitoc" to explore the mitochondrial pathways affected by siNDUFS2. Sorting by adjusted p-value, the first appearing mitochondrial term, "mitochondrial inner membrane" (GO:0005743), is the second of 101 significantly enriched GO terms for the 578 genes uniquely DE between siNDUFS2 and siControl.